

**PERFORMANCE ANALYSIS OF INCLINED MICRO-JET
IMPINGEMENT HEAT TRANSFER IN MICROCHANNEL
USING COMPUTATIONAL FLUID DYNAMICS**

A DISSERTATION

SUBMITTED IN PARTIAL FULFILLMENT OF THE REQUIREMENTS
FOR THE AWARD OF THE DEGREE
OF

**MASTER OF TECHNOLOGY
IN
THERMAL ENGINEERING**

Submitted by:

HIMANSHU RAO BHARTI

(2K21/THE/07)

Under the supervision of

Dr. MOHAMMAD ZUNAID



**DEPARTMENT OF MECHANICAL ENGINEERING
DELHI TECHNOLOGICAL UNIVERSITY**

(Formerly Delhi College of Engineering)

Bawana Road, Delhi-110042

MAY, 2023

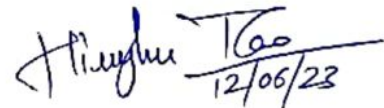
DELHI TECHNOLOGICAL UNIVERSITY
(Formerly Delhi College of Engineering)
Bawana Road, Delhi-110042

CANDIDATE'S DECLARATION

I, HIMANSHU RAO BHARTI, Roll No. 2K21/THE/07 student of M.Tech (Thermal Engineering), hereby declare that the project Dissertation titled "Performance Analysis of Inclined Micro-Jet Impingement Heat Transfer in Microchannel using Computational Fluid Dynamics" which is submitted by me to the Department of Mechanical Engineering, Delhi Technological University, Delhi in partial fulfilment of the requirement for the award of the degree of Master of Technology, is original and not copied from any source without proper citation. This work has not previously formed the basis for the award of any Degree, Diploma Associateship, Fellowship or other similar title or recognition.

Place: Delhi

Date: 12/06/2023



Himanshu Rao
12/06/23

HIMANSHU RAO BHARTI

DEPARTMENT OF MECHANICAL ENGINEERING
DELHI TECHNOLOGICAL UNIVERSITY
(Formerly Delhi College of Engineering)
Bawana Road, Delhi-110042

CERTIFICATE

I hereby certify that the Project Dissertation titled “Performance Analysis of Inclined Micro-Jet Impingement Heat Transfer in Microchannel using Computational Fluid Dynamics” which is submitted by **Himanshu Rao Bharti**, Roll No. **2K21/THE/07**, Department of Mechanical Engineering, Delhi Technological University, Delhi in partial fulfilment of the requirement for the award of the degree of Master of Technology, is a record of the project work carried out by the students under my supervision. To the best of knowledge this work has not been submitted in part or full for any Degree or Diploma to this University or elsewhere.

Place: Delhi

Date: 12/06/2023

Hj Zubon
12/06/23
Dr. **MOHAMMAD ZUNAID**

Asst. Professor

SUPERVISOR

ABSTRACT

The increasing need for efficient cooling methods in electronic chip systems has created a surge in demand for effective solutions to tackle the challenges associated with heat dissipation. This research project focuses on conducting a comprehensive analysis of heat exchange in a microchannel by Computational Fluid Dynamics (CFD) with inclined micro-jet impingement. The aim is to explore the thermal characteristics of hexagonal cross-section jets in order to enhance cooling efficiency for electronic chip applications. The analysis involves the utilization of CFD to solve the steady, incompressible, and laminar flow equations, specifically the Three-Dimensional Navier-Stokes equations. The investigation encompasses various micro-jet arrangements, including parallel and staggered configurations consisting of four, five, nine, thirteen, and sixteen impingements. The jet inclination is maintained at a constant angle of 45 degrees with respect to the impingement surface. The cross-section of the jet nozzle is modelled as a hexagon, with different edge lengths of 60, 80, and 100 microns. The primary objective is to assess and compare the performance of these configurations, gaining valuable insights into their heat transfer capabilities.

The obtained results reveal significant findings regarding the cooling performance. It is observed that the average exit liquid temperature increases as the number of jets in the impingement array increases. This behaviour can be attributed to the increased heat transfer surface area available for dissipation as the number of jets grows. The larger surface area facilitates enhanced convective heat transfer, resulting in a higher average exit liquid temperature. Consequently, the findings suggest that higher jet densities can provide improved cooling performance in electronic chip applications. Among the investigated microjet array configurations, the inclined microjet impingement heat sink with 13 jets demonstrates superior potential compared to other configurations. This particular array design outperforms the rest in terms of its cooling capabilities. The inclined arrangement, coupled with the optimal number of jets, enables the generation of strong impingement forces, facilitating effective heat

transfer at a higher rate. The result is an enhanced convective heat transfer process, leading to a reduction in the average exit liquid temperature.

The research involves the use of CFD simulations using ANSYS Fluent to analyze the cooling performance of the hexagonal cross-section jets. The simulations are conducted to study the effect of various parameters such as Reynolds number, nozzle-to-chip spacing, and jet diameter on the cooling efficiency of the system. The study also includes experimental validation of the simulation results to verify the accuracy of the CFD model. The findings of the study show that the hexagonal cross-section jets significantly improve the cooling performance compared to conventional circular jets. The results indicate that the cooling efficiency is influenced by the geometry of the hexagonal jets, as well as the operating parameters of the system. The research provides insights into the design and optimization of the cooling system for electronic devices using jet impingement, which can potentially enhance the performance and reliability of electronic devices.

ACKNOWLEDGMENT

I would like to express my sincere gratitude to my guide, **Dr. M. Zunaid**, Assistant Professor in the Department of Mechanical Engineering, for his invaluable guidance, support, and expertise throughout the course of this research project. His constant encouragement, insightful feedback, and dedication have been instrumental in shaping the direction and progress of this work. His deep knowledge and passion for the subject have inspired me to strive for excellence and explore new avenues in the field of jet impingement electronic chip cooling.

I would also like to extend my heartfelt appreciation to **Prof. S K Garg**, Head of the Department of Mechanical Engineering, for his support and encouragement. His vision and leadership have provided a conducive environment for academic and research pursuits. I am grateful for his valuable insights and guidance that have contributed to the overall success of this project.

Lastly, I would like to acknowledge my family and friends for their unwavering support, encouragement, and understanding throughout this research endeavour. Their love, belief in my abilities, and motivation have been the driving force behind my perseverance and determination.



HIMANSHU RAO BHARTI

2K21/THE/07

M.Tech (Thermal Engineering)

Delhi Technological University

TABLE OF CONTENTS

CANDIDATE’S DECLARATION	ii
CERTIFICATE	iii
ABSTRACT.....	iv
ACKNOWLEDGMENT.....	vi
TABLE OF CONTENTS.....	vii
LIST OF TABLES	ix
LIST OF FIGURES	xi
NOMENCLATURE.....	xiv
CHAPTER 1	1
INTRODUCTION	1
1.1 BACKGROUND AND MOTIVATION.....	1
1.2 JET IMPINGEMENT COOLING.....	2
1.3 HEXAGONAL CROSS-SECTION JETS	3
1.4 OBJECTIVES OF THE STUDY	4
CHAPTER 2:	5
LITERATURE REVIEW	5
2.1 MICROCHANNEL AND MICROJET IMPINGEMENT COOLING	5
2.2 PREVIOUS STUDIES AND RESEARCH	5
CHAPTER 3:	9
RESEARCH METHODOLOGY.....	9
3.1 RESEARCH OBJECTIVE.....	9
3.2 RESEARCH APPROACH.....	10
3.2.1 Computational Fluid Dynamics (CFD) Simulation.....	10
3.2.2 Physical and Numerical Modelling	10
3.2.3 Assumptions and Boundary conditions	12
3.2.4 Geometry and Mesh Generation.....	13
CHAPTER 4:	46
VALIDATION AND GRID INDEPENDENCE TEST	46
4.1 VALIDATION	46
4.2 GRID INDEPENDENCE TEST	47

CHAPTER 5:	50
RESULTS AND DISCUSSION	50
5.1 Results for E60 Hexagonal Cross-Section Micro-Jets Impingement Heat Sink for Various No. Of Jets.....	51
5.2 Results for E80 Hexagonal Cross-Section Micro-Jets Impingement Heat Sink for Various No. Of Jets.....	54
5.3 Results for E100 Hexagonal Cross-Section Micro-Jets Impingement Heat Sink for Various No. Of Jets.....	57
5.4 Micro-jet design parameters i.e., Edge length and no. of jets effect on the performance of the heat sink	61
CHAPTER 6	64
CONCLUSIONS.....	64
REFERENCES.....	65

LIST OF TABLES

Table 3.1 Geometrical parameters chosen for micro-jet impingent heat sink	13
Table 3.2: Dimensions for E60 hexagonal 4 jets heat sink	16
Table 3.3: Mesh information for E60 hexagonal 4 jets heat sink	17
Table 3.4: Dimensions for E60 hexagonal 5 jets heat sink	18
Table 3.5: Mesh information for E60 hexagonal 5 jets heat sink	19
Table 3.6: Dimensions for E60 hexagonal 9 jets heat sink	20
Table 3.7: Mesh information for E60 hexagonal 9 jets heat sink	21
Table 3.8: Dimensions for E60 hexagonal 13 jets heat sink	22
Table 3.9: Mesh information for E60 hexagonal 13 jets heat sink	23
Table 3.10: Dimensions for E60 hexagonal 16 jets heat sink	24
Table 3.11: Mesh information for E60 hexagonal 16 jets heat sink	25
Table 3.12: Dimensions for E80 hexagonal 4 jets heat sink	26
Table 3.13: Mesh information for E80 hexagonal 4 jets heat sink	27
Table 3.14: Dimensions for E80 hexagonal 5 jets heat sink	28
Table 3.15: Mesh information for E80 hexagonal 5 jets heat sink	29
Table 3.16: Dimensions for E80 hexagonal 9 jets heat sink	30
Table 3.17: Mesh information for E80 hexagonal 9 jets heat sink	31
Table 3.18: Dimensions for E80 hexagonal 13 jets heat sink	32
Table 3.19: Mesh information for E80 hexagonal 13 jets heat sink	33
Table 3.20: Dimensions for E80 hexagonal 16 jets heat sink	34
Table 3.21: Mesh information for E80 hexagonal 16 jets heat sink	35
Table 3.22: Dimensions for E100 hexagonal 4 jets heat sink	36
Table 3.23: Mesh information for E100 hexagonal 4 jets heat sink	37
Table 3.24: Dimensions for E100 hexagonal 5 jets heat sink	38
Table 3.25: Mesh information for E100 hexagonal 5 jets heat sink	39
Table 3.26: Dimensions for E100 hexagonal 9 jets heat sink	40
Table 3.27: Mesh information for E100 hexagonal 9 jets heat sink	41
Table 3.28: Dimensions for E100 hexagonal 13 jets heat sink	42
Table 3.29: Mesh information for E100 hexagonal 13 jets heat sink	43
Table 3.30: Dimensions for E100 hexagonal 16 jets heat sink	44

Table 3.31: Mesh information for E100 hexagonal 16 jets heat sink	45
Table 3.32: Avg. Temp. of solid & liquid interface with respect to mesh size.....	48
Table 4.1: Variation ΔT_{max} , actual & ΔT_{max} , obtained with mass flow rate to calculate % Error.....	47
Table 5.1.1: T_{avg} of contact region of fluid and solid for E60 design	52
Table 5.1.2: T_{avg} of Liquid Channel for E60 design	53
Table 5.2.1: The Avg. temperature of contact region of fluid and solid for E80 design	55
Table 5.2.2: T_{avg} of Liquid Channel for E80 design	56
Table 5.3.1: The Avg. temperature of contact region of fluid & solid for E100 design	58
Table 5.3.2: T_{avg} of Liquid Channel for E100 design	59

LIST OF FIGURES

Fig. 3.1. Schematic diagram of the multiple inclined micro-jet impingements heat sink having hexagonal cross-section jets.	14
Fig. 3.2. Schematic diagram of the inclined micro-jets showing the inclination of 45 degrees with impingement surface.....	14
Fig. 3.3. Various micro-jet arrangements on nozzle plate with an interjet spacing ...	15
Fig. 3.4. Geometry design of inclined hexagonal 4 micro-jets, E60 (a) Ansys SpaceClaim Geometry (b) Geometry indicating inlets & outlet (c) Side view of geometry indicating inlets & outlet.....	16
Fig. 3.5. Meshing of inclined hexagonal 4 hex-jet heat sink, E60.....	17
Fig. 3.6. Geometry design of inclined hexagonal 5 micro-jets, E60 (a) Ansys SpaceClaim Geometry (b) Geometry indicating inlets & outlet (c) Side view of geometry indicating inlets & outlet.....	18
Fig. 3.7. Meshing of inclined hexagonal 5 hex-jet heat sink, E60.....	19
Fig. 3.8. Geometry design of inclined hexagonal 9 micro-jets, E60 (a) Ansys SpaceClaim Geometry (b) Geometry indicating inlets & outlet (c) Side view of geometry indicating inlets & outlet.....	20
Fig. 3.9. Meshing of inclined hexagonal 9 hex-jet heat sink, E60.....	21
Fig. 3.10. Geometry design of inclined hexagonal 13 micro-jets, E60 (a) Ansys SpaceClaim Geometry (b) Geometry indicating inlets & outlet (c) Side view of geometry indicating inlets & outlet.....	22
Fig. 3.11. Meshing of inclined hexagonal 13 hex-jet heat sink, E60.....	23
Fig. 3.12. Geometry design of inclined hexagonal 16 micro-jets, E60 (a) Ansys SpaceClaim Geometry (b) Geometry indicating inlets & outlet (c) Side view of geometry indicating inlets & outlet.....	24
Fig. 3.13 Meshing of inclined hexagonal 16 hex-jet heat sink, E60.....	25
Fig. 3.14: Geometry design of inclined hexagonal 4 micro-jets, E80 (a) Ansys SpaceClaim Geometry (b) Geometry indicating inlets & outlet (c) Side view of geometry indicating inlets & outlet.....	26
Fig. 3.15 Meshing of inclined hexagonal 4 hex-jet heat sink, E80.....	27

Fig. 3.16: Geometry design of inclined 5 hex-jets heat sink, E80 (a) Ansys SpaceClaim Geometry (b) Geometry indicating inlets & outlet (c) Side view of geometry indicating inlets & outlet.....	28
Fig. 3.17 Meshing of inclined hexagonal 5 hex-jets heat sink, E80	29
Fig. 3.18: Geometry design of inclined 9 hex-jets heat sink, E80 (a) Ansys SpaceClaim Geometry (b) Geometry indicating inlets & outlet (c) Side view of geometry indicating inlets & outlet.....	30
Fig. 3.19 Meshing of inclined hexagonal 9 hex-jet heat sink, E80.....	31
Fig. 3.20: Geometry design of inclined 13 hex-jets heat sink, E80 (a) Ansys SpaceClaim Geometry (b) Geometry indicating inlets & outlet (c) Side view of geometry indicating inlets & outlet.....	32
Fig. 3.21 Meshing of inclined hexagonal 13 hex-jet heat sink, E80.....	33
Fig. 3.22: Geometry design of inclined 16 hex-jets heat sink, E80 (a) Ansys SpaceClaim Geometry (b) Geometry indicating inlets & outlet (c) Side view of geometry indicating inlets & outlet.....	34
Fig. 3.23 Meshing of inclined hexagonal 16 hex-jet heat sink, E80.....	35
Fig. 3.24: Geometry design of inclined 4 hex-jets heat sink, E100 (a) Ansys SpaceClaim Geometry (b) Geometry indicating inlets & outlet (c) Side view of geometry indicating inlets & outlet.....	36
Fig. 3.25: Meshing of inclined hexagonal 4 hex-jet heat sink, E100.....	37
Fig. 3.26. Geometry design of inclined 5 hex-jets heat sink, E100 (a) Ansys SpaceClaim Geometry (b) Geometry indicating inlets & outlet (c) Side view of geometry indicating inlets & outlet.....	38
Fig. 3.27. Meshing of inclined hexagonal 5 hex-jet heat sink, E100.....	39
Fig. 3.28. Geometry design of inclined 9 hex-jets heat sink, E100 (a) Ansys SpaceClaim Geometry (b) Geometry indicating inlets & outlet (c) Side view of geometry indicating inlets & outlet.....	40
Fig. 3.29 Meshing of inclined hexagonal 9 hex-jet heat sink, E100.....	41
Fig. 3.30. Geometry design of inclined 13 hex-jets heat sink, E100 (a) Ansys SpaceClaim Geometry (b) Geometry indicating inlets & outlet (c) Side view of geometry indicating inlets & outlet.....	42
Fig. 3.31 Meshing of inclined hexagonal 13 hex-jet heat sink, E100.....	43

Fig. 3.32. Geometry design of inclined 16 hex-jets heat sink, E100 (a) Ansys SpaceClaim Geometry (b) Geometry indicating inlets & outlet (c) Side view of geometry indicating inlets & outlet.....	44
Fig. 3.33 Meshing of inclined hexagonal 16 hex-jet heat sink, E100.....	45
Fig. 4.1.1 Variation ΔT_{max} , actual & ΔT_{max} , obtained with mass flow rate	46
Fig. 4.2.1 Four hexagonal jets model showing inlet and outlet	48
Fig. 4.2.2 Variation of T_{avg} with respect to mesh size selected for simulation	49
Fig. 5.1.1. Temp. Contours at Solid-Liquid Contact Region for E60 Hexagonal Jets (i) 4 hex-jets, (ii) 5 hex-jets, (iii) 9 hex-jets, (iv) 13 hex-jets, (v) 16 hex-jets	52
Fig. 5.1.2. Temperature Contour of Liquid Channel for E60 Hexagonal Jets (i) 4 hex-jets, (ii) 5 hex-jets, (iii) 9 hex-jets, (iv) 13 hex-jets, (v) 16 hex-jets	53
Fig. 5.1.3 Velocity Contour Streamline Distribution for E60 Hexagonal Jets (i) 4 hex-jets, (ii) 5 hex-jets, (iii) 9 hex-jets, (iv) 13 hex-jets, (v) 16 hex-jets	54
Fig. 5.2.1. Temp. Contours at Solid-Liquid Contact Region for E80 Hexagonal Jets (i) 4 hex-jets, (ii) 5 hex-jets, (iii) 9 hex-jets, (iv) 13 hex-jets, (v) 16 hex-jets	55
Fig. 5.2.2. Temperature Contour of Liquid Channel for E80 Hexagonal Jets (i) 4 hex-jets, (ii) 5 hex-jets, (iii) 9 hex-jets, (iv) 13 hex-jets, (v) 16 hex-jets	56
Fig. 5.2.3 Velocity Contour Streamline Distribution for E80 Hexagonal Jets (i) 4 hex-jets, (ii) 5 hex-jets, (iii) 9 hex-jets, (iv) 13 hex-jets, (v) 16 hex-jets	57
Fig. 5.3.1. Temp. Contours at Solid-Liquid Contact Region for E100 Hexagonal (i) 4 hex-jets, (ii) 5 hex-jets, (iii) 9 hex-jets, (iv) 13 hex-jets, (v) 16 hex-jets	58
Fig. 5.3.2. Temperature Contour of Liquid Channel for E100 Hexagonal Jets (i) 4 hex-jets, (ii) 5 hex-jets, (iii) 9 hex-jets, (iv) 13 hex-jets, (v) 16 hex-jets	59
Fig. 5.3.3 Velocity Contour Streamline Distribution for E100 Hexagonal Jets (i) 4 hex-jets, (ii) 5 hex-jets, (iii) 9 hex-jets, (iv) 13 hex-jets, (v) 16 hex-jets	60
Fig. 5.4.1. Variability in temperature at the fluid-solid interface as a function of the number of 45° angled jets.....	62
Fig. 5.4.2. Graph showing pressure variance with changing number of 45° angled Jets.....	62
Fig. 5.4.3. Exit Temperature Fluctuation of Fluid in Relation to Altered Quantity of Angled Jets.....	62

NOMENCLATURE

A_{cs}	Surface area of the substrate base, m^2
C_p	Specific heat at constant pressure, $J\ kg^{-1}\ K^{-1}$
$E60, E80, E100$	Edge length of hexagon, microns
H_c	Height of the channel, metre
H_n	Height of the nozzle
h	Heat transfer coefficient of fluid, $W\ m^{-2}\ K^{-1}$
k	Thermal conductivity of fluid and solid, $W\ m^{-1}\ K^{-1}$
ρ	Density of the fluid, $kg\ m^{-3}$
L_x, L_y, L_z	Length, height and width of the heat sink, respectively, m
n	Number of hexagonal inclined jets
q	Heat flux, $W\ m^{-2}$
$S4a, b; S9a, b;$ $S16a, b;$ $S5a, b; S13a, b$	Interjet spacings of inline 2×2 , 3×3 and 4×4 jet and staggered 5-jet and 13-jet arrays, respectively, m
$T, \Delta T$	Temperature and temperature-rise, respectively, K
$p, \Delta p$	Pressure and pressure drop, respectively, Pa
v	Fluid velocity, $m\ s^{-1}$
x, y, z	Orthogonal coordinate system
Hex-jets	Hexagonal cross-section micro-jets
CFD	Computational Fluid Dynamics
McHS	Microchannel Heat Sink

CHAPTER 1

INTRODUCTION

1.1 BACKGROUND AND MOTIVATION

Electronic chip cooling is a critical aspect of modern technology as electronic devices continue to become more powerful and compact. These devices generate significant amounts of heat during operation, and if not effectively dissipated, this heat can lead to reduced performance, thermal stress, and even irreversible damage. As a result, efficient cooling techniques are essential to ensure optimal chip performance and reliability. One of the primary challenges in electronic chip cooling is the continuous miniaturization and increasing power density of electronic components. As chip sizes decrease and the number of transistors per unit area increases, the heat flux generated within a small space becomes more concentrated. This concentration of heat leads to localized hotspots and temperature gradients, posing a threat to the functionality and longevity of the electronic chip. Consequently, there is a growing demand for efficient cooling techniques that can effectively remove heat from electronic chips. Traditional cooling methods, such as air cooling or heat sinks, often struggle to meet the increasing thermal demands of high-performance chips. As a result, researchers and engineers have been exploring innovative cooling solutions to overcome these challenges.

Jet impingement cooling has emerged as a promising solution due to its ability to provide high heat transfer rates. By directing a high-velocity fluid jet onto the chip surface, jet impingement cooling promotes convective heat transfer, effectively removing heat from the chip. This technique offers several advantages, including efficient heat dissipation, uniform temperature distribution, and the ability to target specific hotspots on the chip.

In this project, the motivation lies in the development and optimization of jet impingement cooling for electronic chips. By utilizing hexagonal cross-section jets, the aim is to enhance the cooling performance and overcome the challenges associated with traditional cooling methods. The investigation focuses on understanding the thermal characteristics of different jet array configurations and their impact on chip cooling efficiency. The project aims to provide insights into the design and optimization of cooling solutions for electronic chips, ultimately improving their performance, reliability, and longevity.

1.2 JET IMPINGEMENT COOLING

Jet impingement cooling is a technique that has garnered significant interest in the field of electronic chip cooling. It involves directing a high-velocity fluid jet onto the surface of the chip, which creates impingement forces that enhance convective heat transfer. The impinging fluid absorbs heat from the chip surface and carries it away, effectively dissipating the thermal energy.

The advantages of jet impingement cooling make it an attractive option for electronic chip cooling applications. Firstly, it offers high heat transfer coefficients, which enable efficient heat dissipation and can effectively address the thermal challenges associated with compact and high-power electronic chips. Additionally, the impingement forces generated by the fluid jet help to break down boundary layer resistances, facilitating enhanced heat transfer. Moreover, jet impingement cooling provides a uniform temperature distribution across the chip surface. This uniformity is achieved by the impingement action, which ensures that the cooling fluid directly interacts with the entire chip area. By minimizing temperature gradients, the risk of localized hotspots and thermal stress-induced failures can be mitigated.

1.3 HEXAGONAL CROSS-SECTION JETS

In this project, hexagonal cross-section jets are utilized to further enhance the cooling efficiency of the jet impingement cooling technique. The choice of hexagonal cross-sections is motivated by their geometric properties, which offer advantages over other cross-sectional shapes.

The hexagonal shape provides a larger surface area compared to circular or rectangular cross-sections, allowing for increased contact area between the cooling fluid and the chip surface. This expanded contact area promotes enhanced convective heat transfer, improving the overall cooling performance. Additionally, the hexagonal cross-sections allow for better fluid flow distribution, minimizing the risk of flow recirculation and aiding in maintaining a uniform temperature profile across the chip. Previous research has demonstrated the benefits of hexagonal cross-section jets in enhancing cooling efficiency in various applications. By leveraging these advantages, this project aims to investigate the thermal characteristics of different jet array configurations with hexagonal cross-section jets and explore their potential for further improving electronic chip cooling.

Overall, the utilization of jet impingement cooling with hexagonal cross-section jets presents an exciting opportunity to address the challenges associated with electronic chip cooling. By combining the benefits of jet impingement cooling and the unique properties of hexagonal cross-sections, this project seeks to contribute to the development of more efficient cooling strategies, ultimately enhancing the performance, reliability, and lifespan of electronic chips.

1.4 OBJECTIVES OF THE STUDY

The primary objectives of this project are to investigate and analyze the performance of inclined micro-jet impingement heat transfer in a microchannel using hexagonal cross-section jets. The specific goals include:

- 1 To examine the thermal characteristics of different jet array configurations: The project aims to investigate five types of jet array configurations consisting of 4, 5, 9, 13, and 16 jets. By varying the number of jets, the study seeks to evaluate their impact on heat transfer and cooling performance. This analysis will provide insights into the optimal jet density for effective heat dissipation.
- 2 To evaluate the influence of jet inclination on heat transfer: The jet inclination angle is maintained at 45 degrees to the impingement surface in this study. By keeping the jet inclination constant, the project aims to assess its effect on convective heat transfer and understand its implications for chip cooling efficiency.
- 3 To explore the impact of hexagonal cross-section jet geometries: The project considers three different edge lengths of the hexagonal cross-section jets, namely 60, 80, and 100 microns. By varying the jet geometry, the study aims to examine how the cross-sectional shape and size influence heat transfer characteristics and overall cooling performance.

CHAPTER 2:

LITERATURE REVIEW

The literature review in this chapter aims to provide a comprehensive overview of previous studies and research related to jet impingement cooling, hexagonal cross-section jets, and electronic chip cooling. By reviewing the existing body of knowledge, this section establishes a foundation for the current study and identifies the research gaps that this project aims to address. The review encompasses key findings, methodologies, and insights gained from relevant literature sources.

2.1 MICROCHANNEL AND MICROJET IMPINGEMENT COOLING

Microchannel cooling is another technique that has gained attention in electronic chip cooling due to its potential for high heat transfer rates and compact design. Research studies have investigated the thermal performance of microchannels, including their geometric configurations, flow characteristics, and heat transfer mechanisms. These studies have explored different channel designs, such as rectangular, circular, and triangular cross-sections, to optimize heat transfer and minimize pressure drop. Additionally, investigations have been conducted on the effects of varying channel dimensions, surface enhancements, and flow conditions. The findings from these studies contribute to the understanding of microchannel cooling and provide insights for the current project.

2.2 PREVIOUS STUDIES AND RESEARCH

It is suggested that microchannels and microjet impingements could be used as feasible methods for managing electronics' hot spots and removing surface heat. Because of improvements in packaging and smaller electronics, it is now very challenging for the scientific researchers to decrease the size of the heat sink and

increase the rate of the heat removal method. These small electronics releases an excessive amount of heat flux because of the tiny chip size and greater transistor density. The failure of the electronics may result from the package degrading and the chip temperature exceeding its usual operating temperature if the heat at the chip surface is not effectively removed.

In comparison to conventional channels, microchannels offer lower heat transfer resistance due to their smaller scale. Tuckerman and Pease [1] were among one of the researchers who examined fluid flow micro-channel heat sinks. They succeeded in conducting experiments on three micro-channels with dimensions of 50, 55, and 56 μm and 287, 302, and 320 μm , respectively, and created a novel theory of micro-cooling for scientists. A heat flow of up to 790 W/cm^2 could be removed by one of the heat sinks. Yeh [2] studied into the degree to which the microchannel's design factors can substantially impact the flow Reynolds number and the rate of heat transfer. Garimella and Rice [3] propose that the rate of heat transfer improves with increasing fluid flow Reynolds number and nozzle area in microchannels. Additionally, the utilization of micro-jet impingements on substrates has been recently suggested as a means to control hot spots in electronics and enhance temperature uniformity [4, 5]. Wu et al. [4] conducted experimental research on the heat transfer behaviour of single jets measuring 500 and 550 μm , as well as a jet array with varying hydraulic diameters (H_c) ranging from 200 to 3,000 μm . At a pressure drop of approximately 34,474 Pa, they were able to attain the area-averaged heat transfer coefficient for a single jet with a thickness of 500 μm and a height of 750 μm is 320 $\text{W}/\text{m}^2\text{K}$. Additionally, they noted that cooling efficiency was higher at lower driving pressures and fell as driving pressure increased. The comparison of jet impingement cooling with micro-channels was done by Lee and Vafai [5]. They came to the conclusion that jet impingement is equivalent to or better than micro-channel cooling for a large target plate with a good arrangement of spent flow after impingements, while micro-channel cooling is superior for a heated surface smaller than 70 mm \times 70 mm. Peng and Peterson [6] and Foli et al. [7] analyzed microchannels and found that the convective heat transfer is influenced by both the design factors and inlet factors of the microchannels. Mala et al. [8] state that estimating the heat rate transmission in a complicated microchannel geometry poses significant challenge. Several authors used curved and zigzag microchannels [9-13] and passive frameworks inside of the

microchannels [14,15] in an effort to improve performance by minimising resistance and pressure loss in a McHS. Additional research was done to examine how nanofluids might be used to reduce temperature gradients and resistance to heat transmission as well as to remove more heat from chip surfaces [16–21].

At the beginning of the microchannel, which stretches in the direction of the flow, thermal and hydrodynamic boundary layers are developed. Additionally, it thickens upstream as the flow continues. In the downstream path, thermal resistance is consequently decreased. To improve performance, it was suggested that the boundary layer generation process be disrupted and the flow be made chaotic. By applying the theory of jet impingement, Wu et al. [22] and Lee and Vafai [23] were able to produce this boundary layer, disturb the flow, and see improvement in heat transmission. Fedorov and Viskanta [24] came to the conclusion that the micro channel exhibits complicated heat flow patterns and that average temperature is not a authentic indicator of the direction of heat flow. Thermal stresses are caused by a further significant temperature difference and hence have an impact on things like electronics. According to several studies, the fluid temperature rises throughout the channel's length [25,26], and the pressure loss in the channel gets higher as velocity increases [27,28]. Husain and Kim's study [29] found that as fluid velocity in the channel advances, thermal resist ability within the microchannel lowers. The writers also used parametric optimisation to determine how design parameters affected fluid power, pressure loss, and thermal performance. The possibility of microjet impingement heat sinks was investigated further. In studies on single-phase heat transfer, Michna et al. [30] recorded the stagnation phenomenon. Further curve fitting was done to get correlations for the Nusselt number, and they came to the conclusion that there was little relationship between the two numbers. Husain et al. [31] investigated a parametric study on multi-jet impingements, where they examined various multi-jet configurations and reported a range of heat transfer coefficients, pressure losses, module resistances, and required power. They discovered that the stand-off, or the gap that exists between the impingement surface and the jet opening, has a considerable impact on the rate of heat transfer. Paz and Jubran [32] observed that decreasing the stand-off results in an increase in heat transport. Husain et al. [33] performed numerical research and optimized non-dimensional geometric variables to achieve the lowest module resistance and fluid power possible.

Muszynski and Andrzejczyk [34] conducted experiments on a hybrid microchannel microjet module to take the benefit of the boundary layer slimming brought on by the impingements. In contrast to microchannels, the jet impingement was discovered to be the predominant mechanism of heat transport. Husain et al. [35] introduced a hybrid notion that combines passive structures with microjets within a microchannel. The performance of the suggested hybrid idea is superior to that of passive structures or microjets in a microchannel, according to the authors' comparison of various configurations of passive structures and microjets. Naphon et al. [36] utilized a pin-fin heat sink module featuring a central jet inlet and four outlets positioned at the corners of the McHS (Microchannel Heat Sink) in their experimental and numerical investigation of the hybrid idea. The authors use cooling nanofluid to further improve heat transfer. Kempers et al. [37] put forth the proposal of an integrated hybrid pin-fin Microchannel Heat Sink (McHS) incorporating microjets. The performance attributes were supplied by the writers. Similar tendencies can be seen in experimental and CFD features. However, a sizable divergence between CFD predictions and experimental data was seen. Peng et al. [38] recommended the utilization of slot jet impingement with alternative extraction slots. To understand the parametric impact of geometric design factors, the authors performed a numerical analysis.

The aforementioned references represent a selection of studies that have contributed significantly to the understanding of jet impingement cooling, hexagonal cross-section jets, and electronic chip cooling. These works provide valuable insights into the performance, optimization, and applications of these cooling techniques. By reviewing and analyzing these studies, this project aims to build upon the existing knowledge and contribute further to the field of electronic chip cooling.

CHAPTER 3:

RESEARCH METHODOLOGY

3.1 RESEARCH OBJECTIVE

The research objective of this study is to investigate the thermal characteristics such as average temperature of solid-liquid interface, average temperature of outlet, and changes in pressure as the number of jets increases of inclined micro-jet impingement heat transfer in microchannels using hexagonal cross-section jets. The study aims to analyze the heat transfer performance, temperature distribution, and flow characteristics of different jet array configurations and jet geometries. The specific objectives of the research are as follows:

1. To evaluate how the quantity of jets affects the efficiency of heat transmission. We will study five distinct jet array configurations with 4, 5, 9, 13, and 16 jets.
2. To examine the influence of jet geometry on the thermal characteristics. The jet cross-section will be taken as a hexagon with different edge lengths of 60, 80, and 100 microns.
3. To investigate the effect of jet inclination on the heat transfer performance. The jet inclination angle will be kept constant at 45 degrees to the impingement surface.
4. To determine the average solid-liquid interface temperature and average exit liquid temperature, and their correlation with the number of jets in the array. The results will help identify the optimal jet array configuration for enhanced cooling.
5. To evaluate the potential of inclined microjet impingement heat sink with optimal jet array compared to other microjet array configurations. The analysis will

consider the heat transfer performance, temperature distribution, and flow characteristics.

6. To use laminar flow modelling in the simulations, as the flow is expected to remain within the laminar regime for the given flow rates.
7. To apply a constant heat flux of 25 W/cm^2 on the solid substrate, assuming it is made of silicon.
8. To maintain a constant mass flow rate of $1.45 \times 10^{-4} \text{ kg/s}$ for the working fluid water liquid.
9. To analyze the average temperature rise and pressure drop for all configurations, evaluating the thermal performance and assessing the influence of the different parameters.

3.2 RESEARCH APPROACH

To achieve the research objective, the following research approach will be adopted:

3.2.1 Computational Fluid Dynamics (CFD) Simulation

The research will utilize CFD simulations to analyze the thermal performance of the micro-jet impingement cooling system. CFD provides a powerful tool to simulate fluid flow, heat transfer, and turbulence phenomena. The simulations will be performed using commercial CFD software, such as ANSYS Fluent, which can accurately model and predict the behaviour of fluid flow and heat transfer in complex geometries.

3.2.2 Physical and Numerical Modelling

In this research, the simulations will assume laminar flow conditions since the flow within the microchannels is expected to remain in the laminar regime due to

the relatively low flow rates considered. Laminar flow is characterized by smooth and ordered fluid motion, which is appropriate for the analysis of micro-jet impingement heat transfer.

The governing equations for the fluid flow and heat transfer in the microchannels will be the 3D Navier-Stokes equations, which describe the conservation of mass, momentum, and energy for incompressible fluid flow and conjugate heat transport in the model. The micro-nozzles and conduit were cooled by using water. These equations will be solved numerically using a suitable solver in the chosen computational fluid dynamics (CFD) software. The governing equations can be written in partial differential form as follows: [39]

$$\frac{\partial(\rho_f v_i)}{\partial x_i} = 0 \quad (1)$$

$$\frac{\partial(\rho_f v_i v_j)}{\partial x_i} = -\frac{\partial p}{\partial x_i} + \frac{\partial}{\partial x_j} \left(u_f \frac{\partial v_i}{\partial x_j} \right) + \frac{\partial}{\partial x_j} \left(\mu_f \frac{\partial v_j}{\partial x_i} \right) - \frac{2}{3} \frac{\partial}{\partial x_i} \left(\mu_f \frac{\partial v_k}{\partial x_k} \right) \quad (2)$$

$$\frac{\partial(\rho_f v_j c_p T_f)}{\partial x_j} = v_j \frac{\partial p}{\partial x_j} \left(k_f \frac{\partial T_f}{\partial x_i} \right) + \tau_{ij} \frac{\partial u_j}{\partial x_i} \quad (3)$$

(For the fluid)

$$\frac{\partial}{\partial x_j} \left(k_s \frac{\partial T_s}{\partial x_j} \right) = 0 \quad (\text{For the substrate conduction}) \quad (4)$$

The flow field is provided through simulation in ANSYS Fluent. It was completed while different fluids were flowing through it. The simulation defines a computational fluid domain using a simple, produced hexahedral mesh. Solid and fluid domains are conjugately categorised throughout iteration.

Hexahedral mesh was advised for a certain computational domain during fluid flow. For the purpose of the study, the fluid wall in the fluid domain was optimised with the exception of the solid fluid domain interface, which was kept adiabatic.

It is assumed that there is no slip condition ($v=0$) at the solid-fluid interface in a channel where homogeneous heat flux is given from the solid substrate base towards the cooling fluid. The interior wall of the nozzle continued to be inclined from the top surface of the channel during the whole flow.

HEAT FLUX EQUATION:

$$\frac{Q}{A} = h \times (T_2 - T_1) \quad (5)$$

$$q = h \times (T_2 - T_1) \quad (6)$$

NUSSELT NO.:

$$Nu = \frac{hD_c}{k} \quad (7)$$

HEAT TRANSFER COEFFICIENT:

$$h = \frac{q}{(T_2 - T_1)} \quad (8)$$

CHARACTERISTICS DIAMETRE:

$$D_c = \frac{4A}{P} \quad (9)$$

$$\text{Area} = \text{Height} \times \text{Breadth} \quad (10)$$

$$P = 2 \times (\text{Height} + \text{Breadth}) \quad (11)$$

ENERGY CARRIED BY THE FLOWING FLUID:

$$Q = m C_p \Delta T \quad (12)$$

$$M = \rho V \quad (13)$$

3.2.3 Assumptions and Boundary conditions

1. At the channel's entrance, uniform inlet temperature and static pressure were provided.
2. All surfaces are considered to be adiabatic, and there is no slip condition imposed between the solid and fluid interface domain.
3. In the fluid and solid domain interfaces, temperature is taken to remain constant.
4. The channel's outlet is determined by the mass flow rate.

3.2.4 Geometry and Mesh Generation

Fig. 3.1 shows a schematic diagram of silicon-based multiple micro-jet impingements heat sink model that was designed on the reverse of the microchip with multiple nozzles. The area of the microchannel substrate is $11 \times 11 \text{ mm}^2$. The impingement heat sink plate has a total thickness of 0.8 mm. The nozzles were made on the substrate, and a water channel was built to enable liquid to flow through the nozzles. While the nozzles with a fluid channel and substrate base were included in the computational area, the substrate on which these nozzles were constructed was not analyzed for conservative analysis. The substrate's outlet channel and jets were made separately and then joined with epoxy to create the desired structure.

Table 3.1 Geometrical parameters chosen for micro-jet impingent heat sink

Geometrical Parameter	Value
Thickness of the silicon substrate (T_s)	100 μm
Height of the channel (H_c)	300 μm
Height of the nozzle plate (H_n)	400 μm
Edge lengths of hexagonal cross section jets (E)	60, 80, 100 μm
Number of jets	4, 5, 9, 13, 16

As depicted in Fig. 3.1, the liquid jets interact with heated surface, the flow shifts to a radial direction while removing heat content from the surface, and it eventually reaches the output port. 45° inclination of jets with respect to impingement surface is shown in Fig. 3.2.

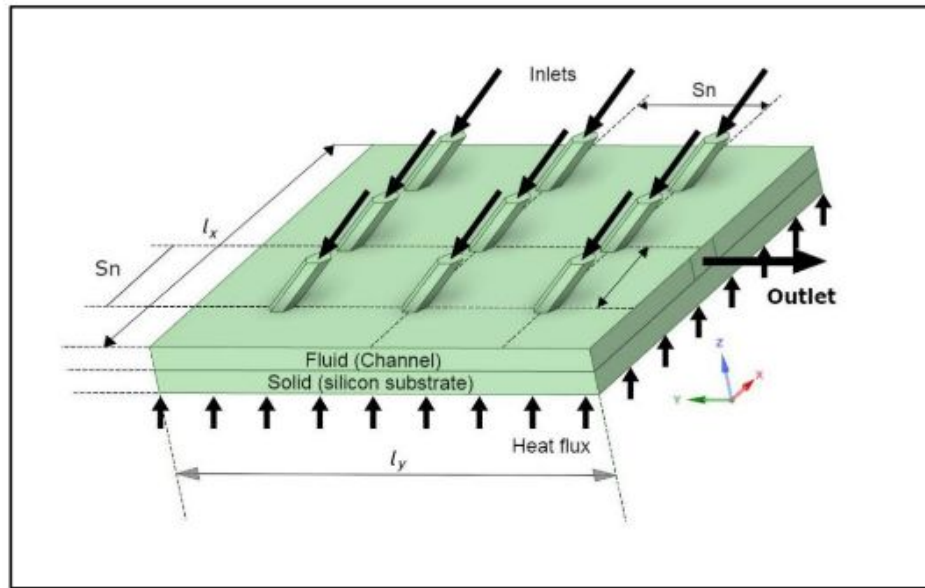


Fig. 3.1. Schematic diagram of the multiple inclined micro-jet impingements heat sink having hexagonal cross-section jets.

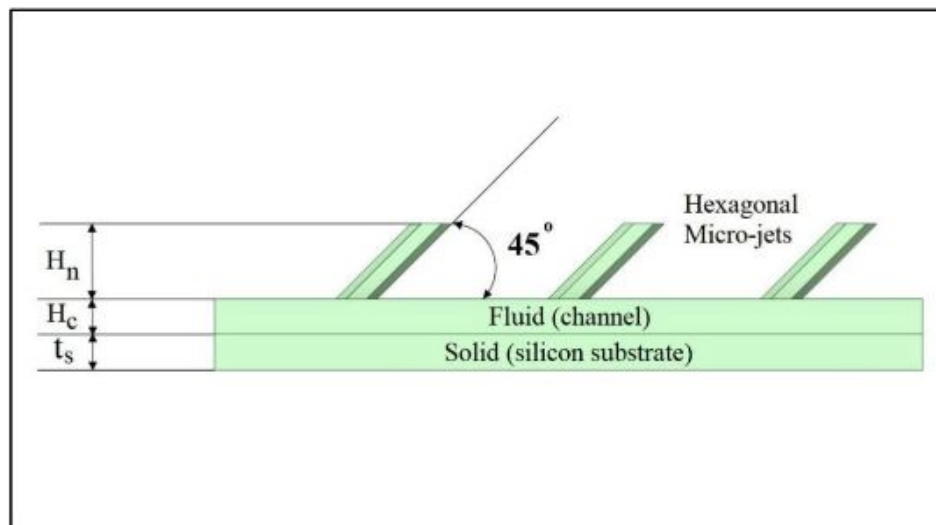


Fig. 3.2. Schematic diagram of the inclined micro-jets showing the inclination of 45 degrees with impingement surface.

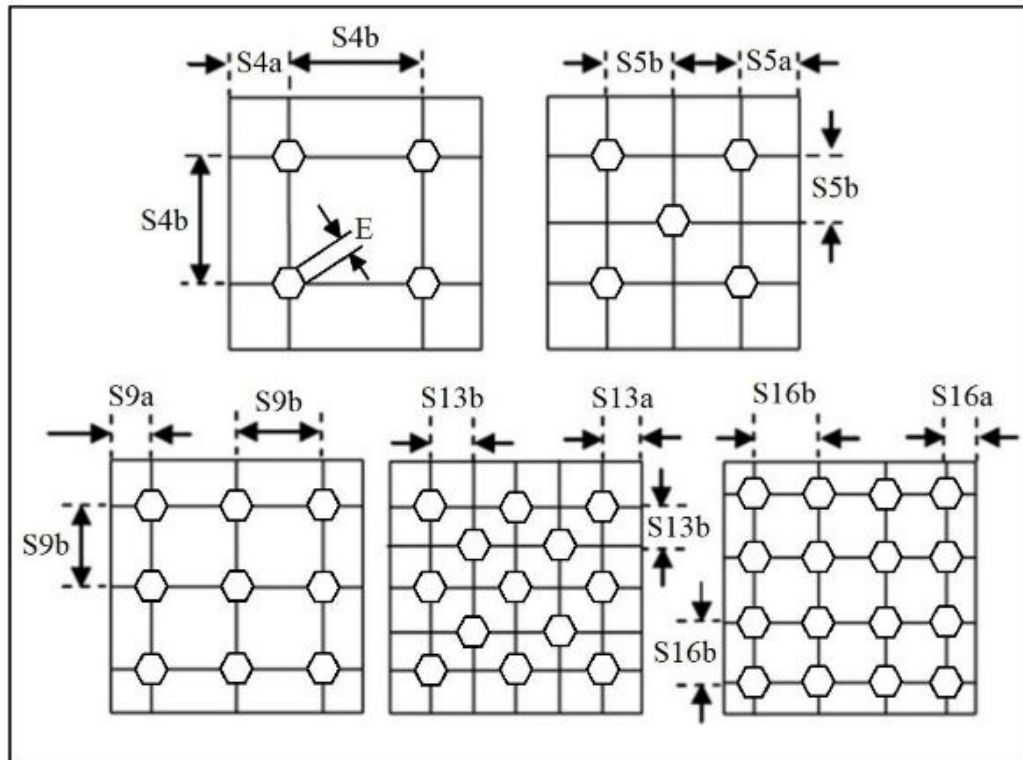


Fig. 3.3. Various micro-jet arrangements on nozzle plate with an interjet spacing, $S_{4a} = 2.75$ mm, $S_{4b} = 5.5$ mm; $S_{5a} = 2.75$ mm, $S_{5b} = 2.75$ mm; $S_{9a} = 1.75$ mm, $S_{9b} = 3.75$ mm; $S_{13a} = 1.5$ mm, $S_{13b} = 2$ mm; $S_{16a} = 1.375$ mm, $S_{16b} = 2.75$ mm.

To solve these CFD problems, the geometry model of the inclined hexagonal micro-jet impingement heat sink was designed using ANSYS SpaceClaim, and then meshing and CFD simulations are done using ANSYS Fluent.

Total of 15 geometries were made of hexagonal cross-section having edge lengths of 60, 80 and 100 microns for 4, 5, 9, 13 & 16 inclined jets each. All the geometries were simulated on ANSYS Workbench. Following are the details of the geometries.

Geometry 1 is considered for simulation which is 45° inclined 4 hexagonal cross-section jets of edge length 60 microns. Table 3.2 shows the dimensions parameters of the 4 hex-jets model. Fig. 3.4 presents different views of the geometry showing inlets and outlet. Table 3.3 provides the mesh information considered for simulation. Fig 3.5 represents the meshing of the 4 hex-jets model.

Geometry 1 : 45° inclined 4 micro-jets, E60

Table 3.2: Dimensions for E60 hexagonal 4 jets heat sink

A_{cs} (mm ²)	T_s (μ m)	H_c (μ m)	E (μ m)	H_n (μ m)	S_n (μ m)
11×11	100	300	60	40	5500

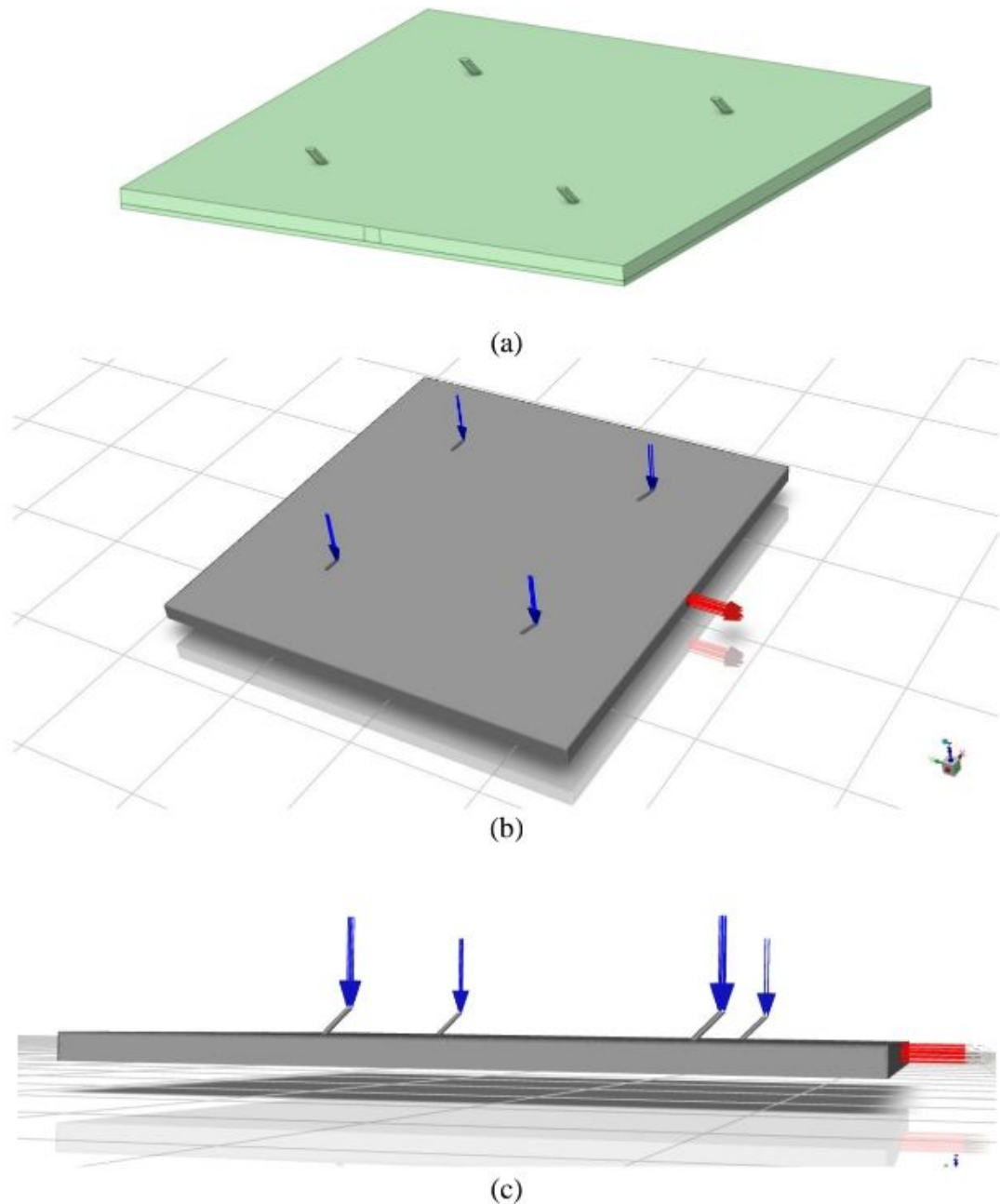


Fig. 3.4. Geometry design of inclined hexagonal 4 micro-jets, E60 (a) Ansys SpaceClaim Geometry (b) Geometry indicating inlets & outlet (c) Side view of geometry indicating inlets & outlet

Table 3.3: Mesh information for E60 hexagonal 4 jets heat sink

Physics solved by	CFD
Solver used	Fluent
Element order	Linear
Curvature Proximity	On
Smoothing	Medium
Element size	5.e-005 m
Nodes	777471
Elements	2049094

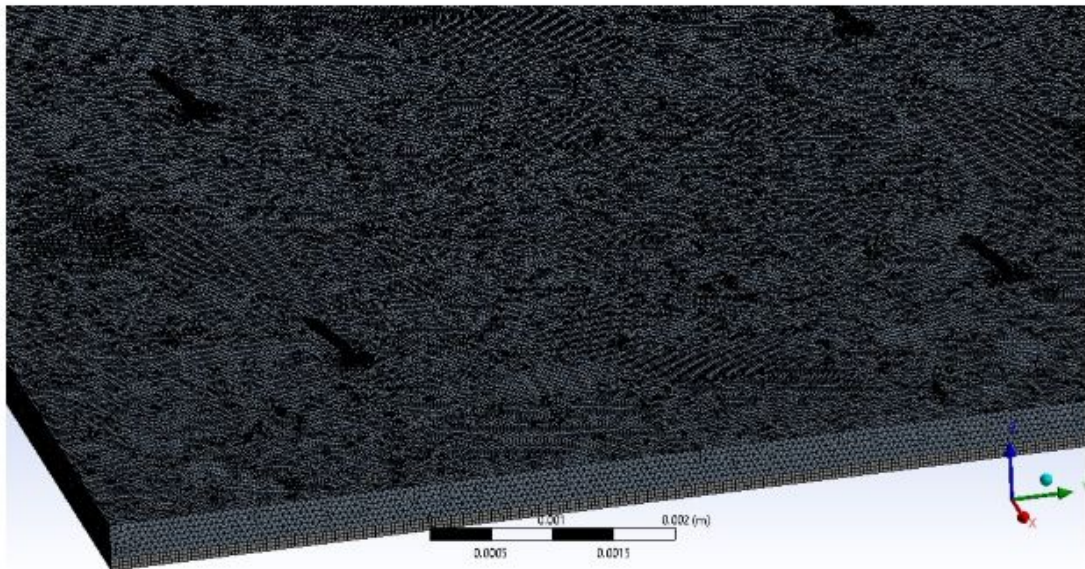


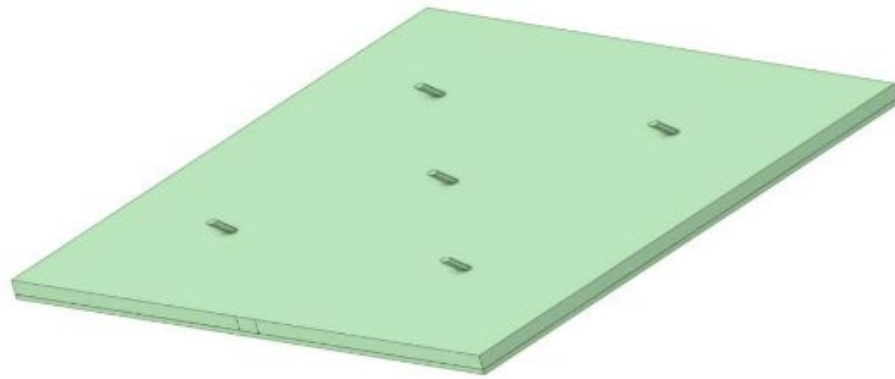
Fig. 3.5. Meshing of inclined hexagonal 4 hex-jet heat sink, E60

Geometry 2 is considered for simulation which is 45° inclined 5 hexagonal cross-section jets of edge length 60 microns. Table 3.4 shows the dimensions parameters of the 5 hex-jets model. Fig. 3.6 presents different views of the geometry showing inlets and outlet. Table 3.5 provides the mesh information considered for simulation. Fig. 3.7 represents the meshing of the 5 hex-jets E60 model.

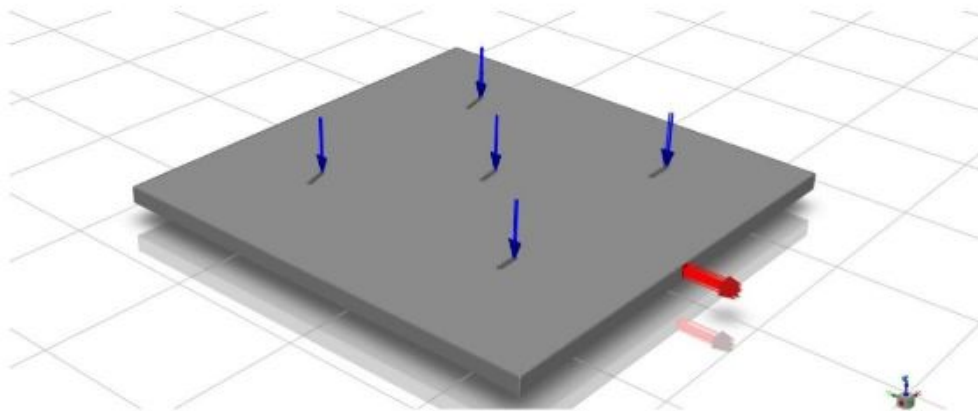
Geometry 2 : 45° inclined 5 micro-jets, E60

Table 3.4: Dimensions for E60 hexagonal 5 jets heat sink

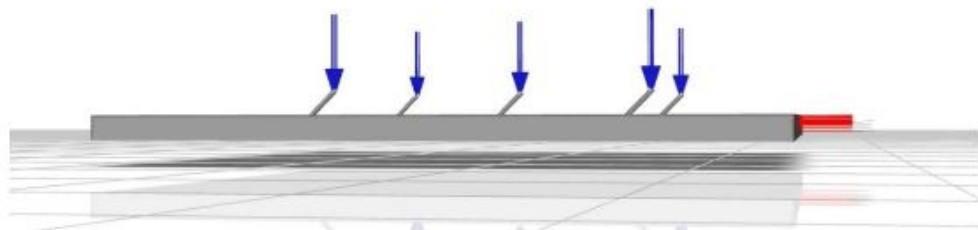
A_{cs} (mm ²)	T_s (μ m)	H_c (μ m)	E (μ m)	H_n (μ m)	S_n (μ m)
11×11	100	300	60	40	2750



(a)



(b)



(c)

Fig. 3.6. Geometry design of inclined hexagonal 5 micro-jets, E60 (a) Ansys SpaceClaim Geometry (b) Geometry indicating inlets & outlet (c) Side view of geometry indicating inlets & outlet

Table 3.5: Mesh information for E60 hexagonal 5 jets heat sink

Physics solved by	CFD
Solver used	Fluent
Element order	Linear
Curvature Proximity	On
Smoothing	Medium
Element size	5.e-005 m
Nodes	778463
Elements	2053019



Fig. 3.7. Meshing of inclined hexagonal 5 hex-jet heat sink, E60

Geometry 3 is considered for simulation which is 45° inclined 9 hexagonal cross-section jets of edge length 60 microns. Table 3.6 shows the dimensions parameters of the 9 hex-jets model. Fig. 3.8 presents different views of the geometry showing inlets and outlet. Table 3.7 provides the mesh information considered for simulation. Fig. 3.9 represents the meshing of the 9 hex-jets E60 model.

Geometry 3 : 45° inclined 9 micro-jets, E60

Table 3.6: Dimensions for E60 hexagonal 9 jets heat sink

A_{cs} (mm ²)	T_s (μ m)	H_c (μ m)	E (μ m)	H_n (μ m)	S_n (μ m)
11×11	100	300	60	40	3750

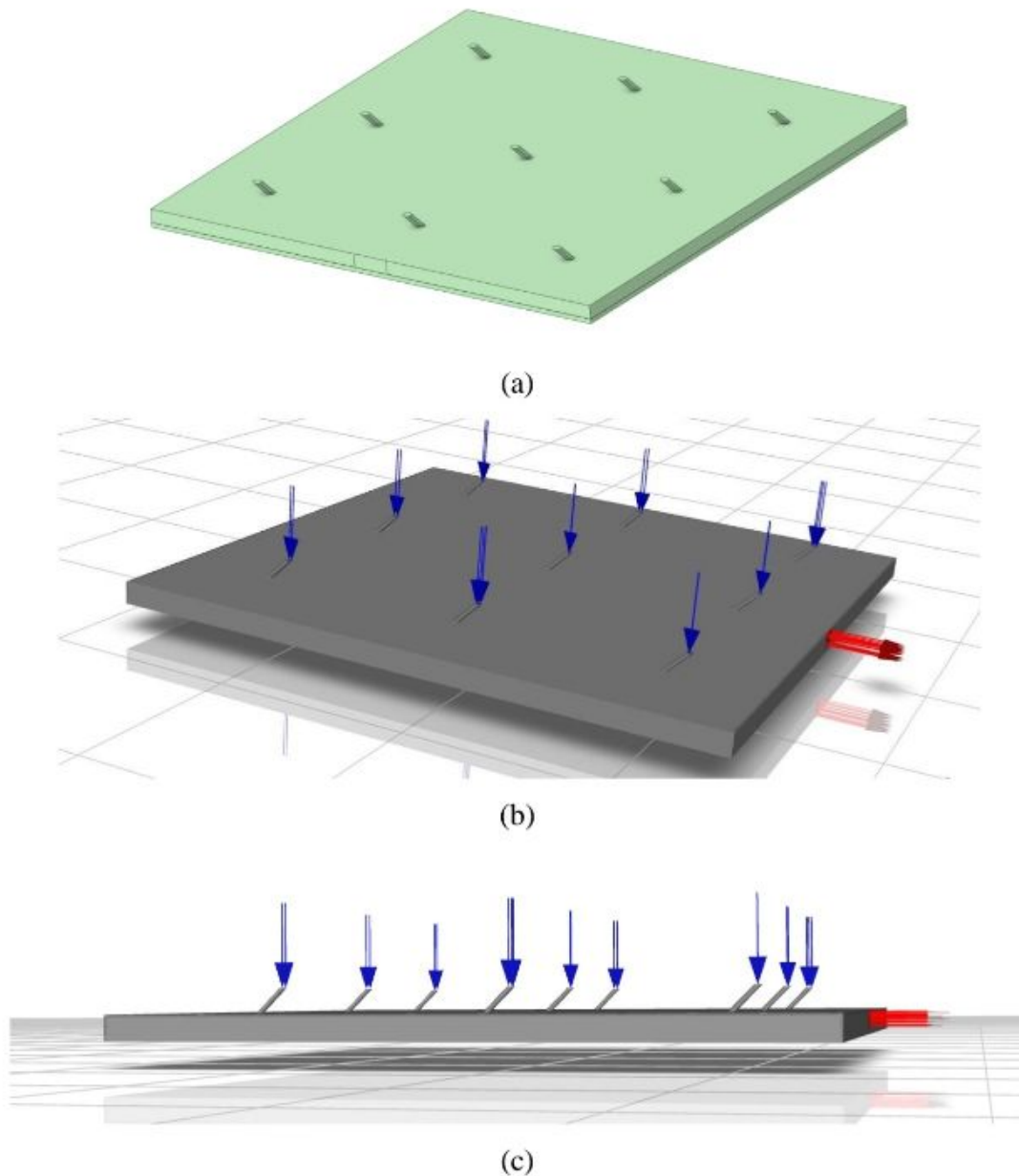


Fig. 3.8. Geometry design of inclined hexagonal 9 micro-jets, E60 (a) Ansys SpaceClaim Geometry (b) Geometry indicating inlets & outlet (c) Side view of geometry indicating inlets & outlet

Table 3.7: Mesh information for E60 hexagonal 9 jets heat sink

Physics solved by	CFD
Solver used	Fluent
Element order	Linear
Curvature Proximity	On
Smoothing	Medium
Element size	5.e-005 m
Nodes	783222
Elements	2100635

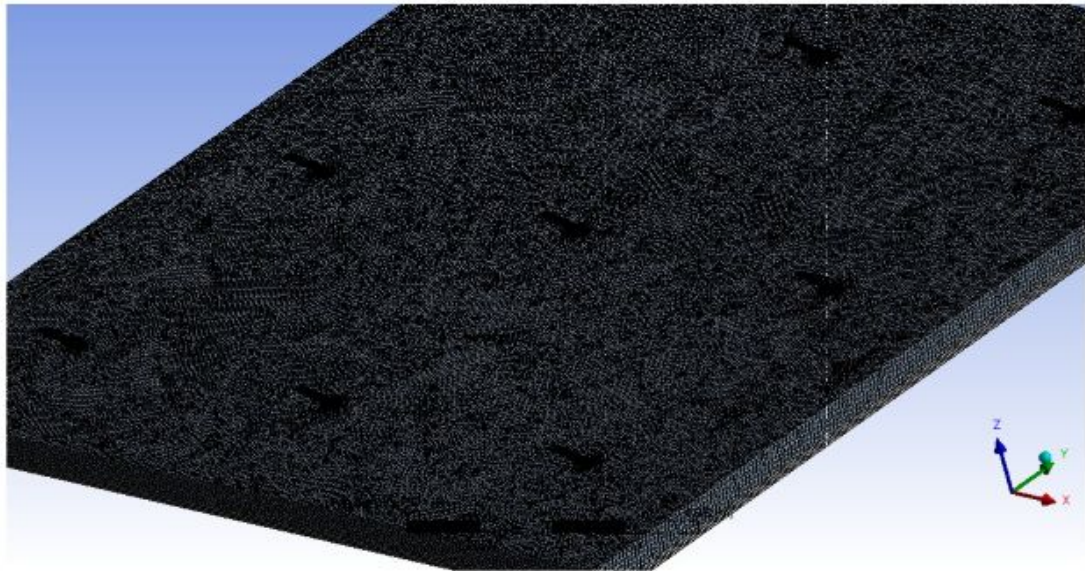


Fig. 3.9. Meshing of inclined hexagonal 9 hex-jet heat sink, E60

Geometry 4 is considered for simulation which is 45° inclined 13 hexagonal cross-section jets of edge length 60 microns. Table 3.8 shows the dimensions parameters of the 13 hex-jets model. Fig. 3.10 presents different views of the geometry showing inlets and outlet. Table 3.9 provides the mesh information considered for simulation. Fig. 3.11 represents the meshing of the 13 hex-jets E60 model.

Geometry 4 : 45° inclined 13 micro-jets, E60

Table 3.8: Dimensions for E60 hexagonal 13 jets heat sink

A_{cs} (mm ²)	T_s (μ m)	H_c (μ m)	E (μ m)	H_n (μ m)	S_n (μ m)
11×11	100	300	60	40	2000

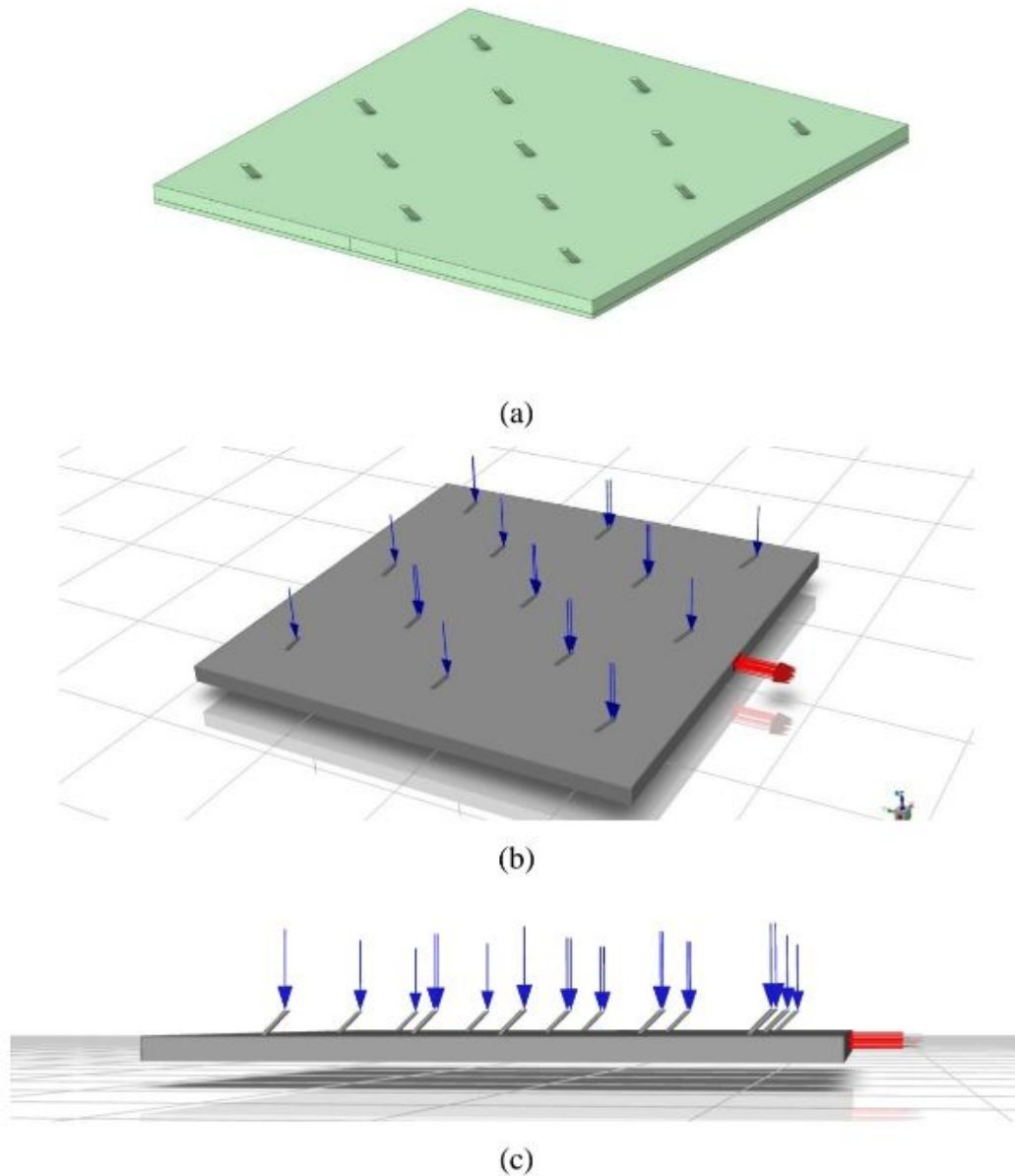


Fig. 3.10. Geometry design of inclined hexagonal 13 micro-jets, E60 (a) Ansys SpaceClaim Geometry (b) Geometry indicating inlets & outlet (c) Side view of geometry indicating inlets & outlet

Table 3.9: Mesh information for E60 hexagonal 13 jets heat sink

Physics solved by	CFD
Solver used	Fluent
Element order	Linear
Curvature Proximity	On
Smoothing	Medium
Element size	5.e-005 m
Nodes	789572
Elements	2100635

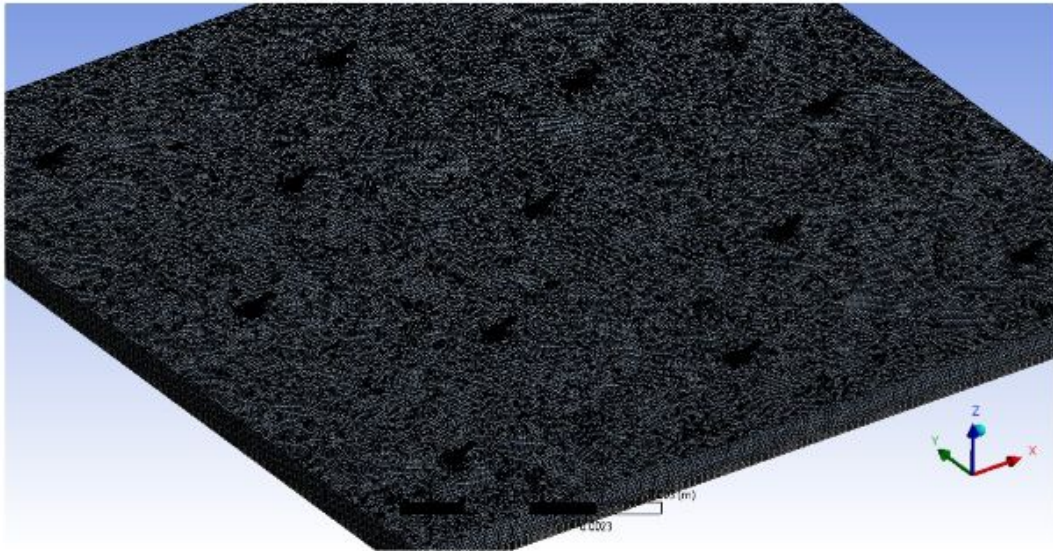


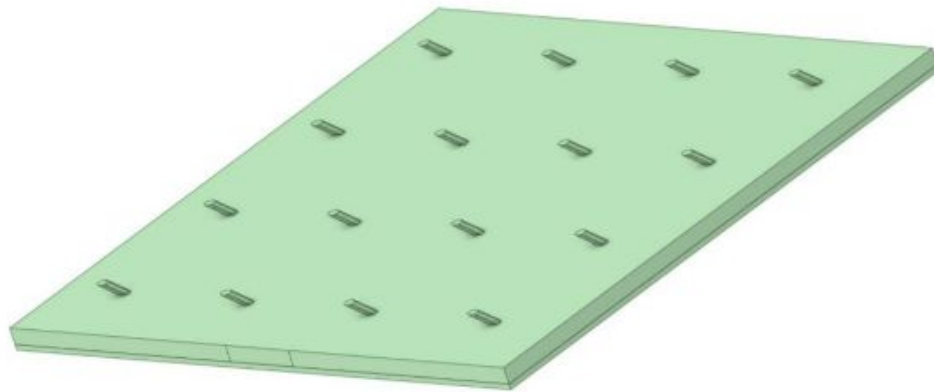
Fig. 3.11. Meshing of inclined hexagonal 13 hex-jet heat sink, E60

Geometry 5 is considered for simulation which is 45° inclined 16 hexagonal cross-section jets of edge length 60 microns. Table 3.10 shows the dimensions parameters of the 16 hex-jets model. Fig. 3.12 presents different views of the geometry showing inlets and outlet. Table 3.11 provides the mesh information considered for simulation. Fig. 3.13 represents the meshing of the 16 hex-jets E60 model.

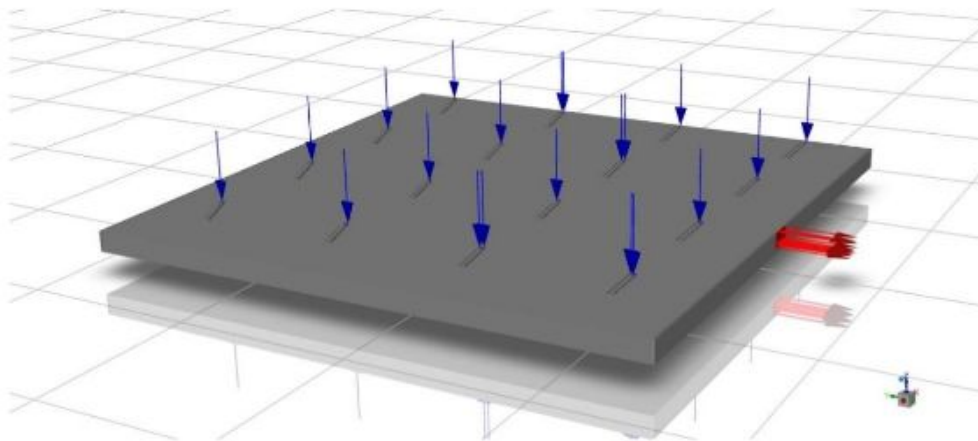
Geometry 5 : 45° inclined 16 micro-jets, E60

Table 3.10: Dimensions for E60 hexagonal 16 jets heat sink

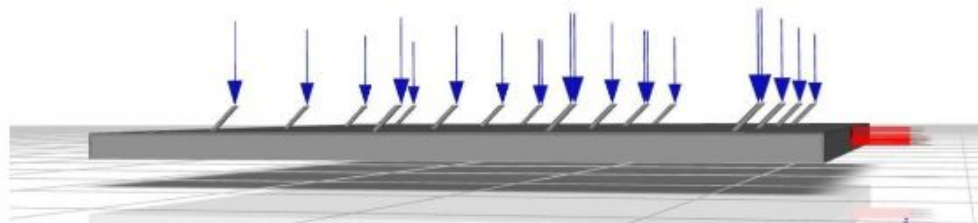
A_{cs} (mm ²)	T_s (μ m)	H_c (μ m)	E (μ m)	H_n (μ m)	S_n (μ m)
11×11	100	300	60	40	2750



(a)



(b)



(c)

Fig. 3.12. Geometry design of inclined hexagonal 16 micro-jets, E60 (a) Ansys SpaceClaim Geometry (b) Geometry indicating inlets & outlet (c) Side view of geometry indicating inlets & outlet

Table 3.11: Mesh information for E60 hexagonal 16 jets heat sink

Physics solved by	CFD
Solver used	Fluent
Element order	Linear
Curvature Proximity	On
Smoothing	Medium
Element size	5.e-005 m
Nodes	793981
Elements	2120141

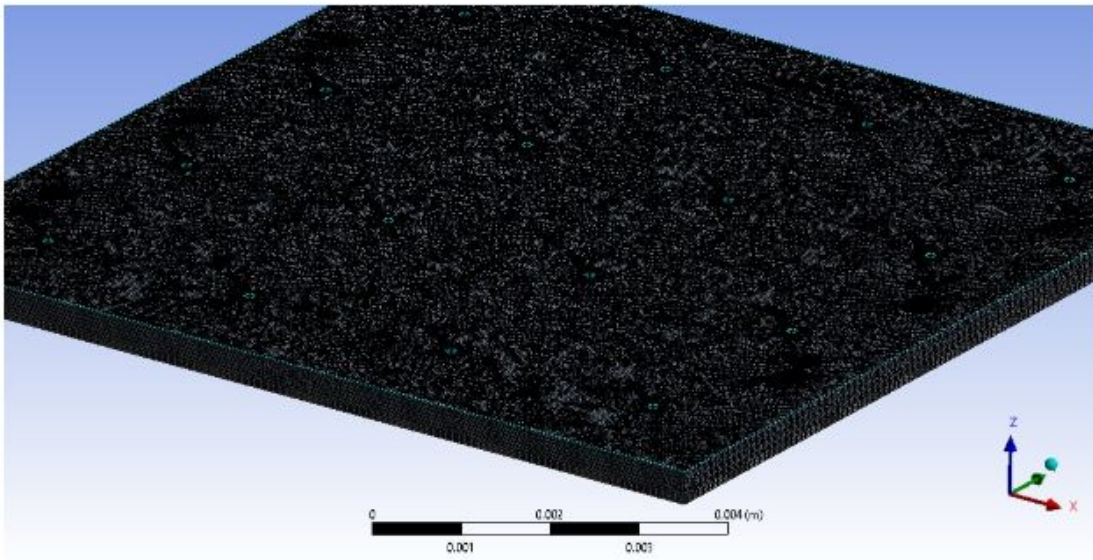


Fig. 3.13 Meshing of inclined hexagonal 16 hex-jet heat sink, E60

Geometry 6 is considered for simulation which is 45° inclined 4 hexagonal cross-section jets of edge length 80 microns. Table 3.12 shows the dimensions parameters of the 4 hex-jets model. Fig. 3.14 presents different views of the geometry showing inlets and outlet. Table 3.13 provides the mesh information considered for simulation. Fig. 3.15 represents the meshing of the 4 hex-jets E80 model.

Geometry 6 : 45° inclined 4 micro-jets, E80

Table 3.12: Dimensions for E80 hexagonal 4 jets heat sink

A_{cs} (mm ²)	T_s (μ m)	H_c (μ m)	E (μ m)	H_n (μ m)	S_n (μ m)
11×11	100	300	60	40	5500

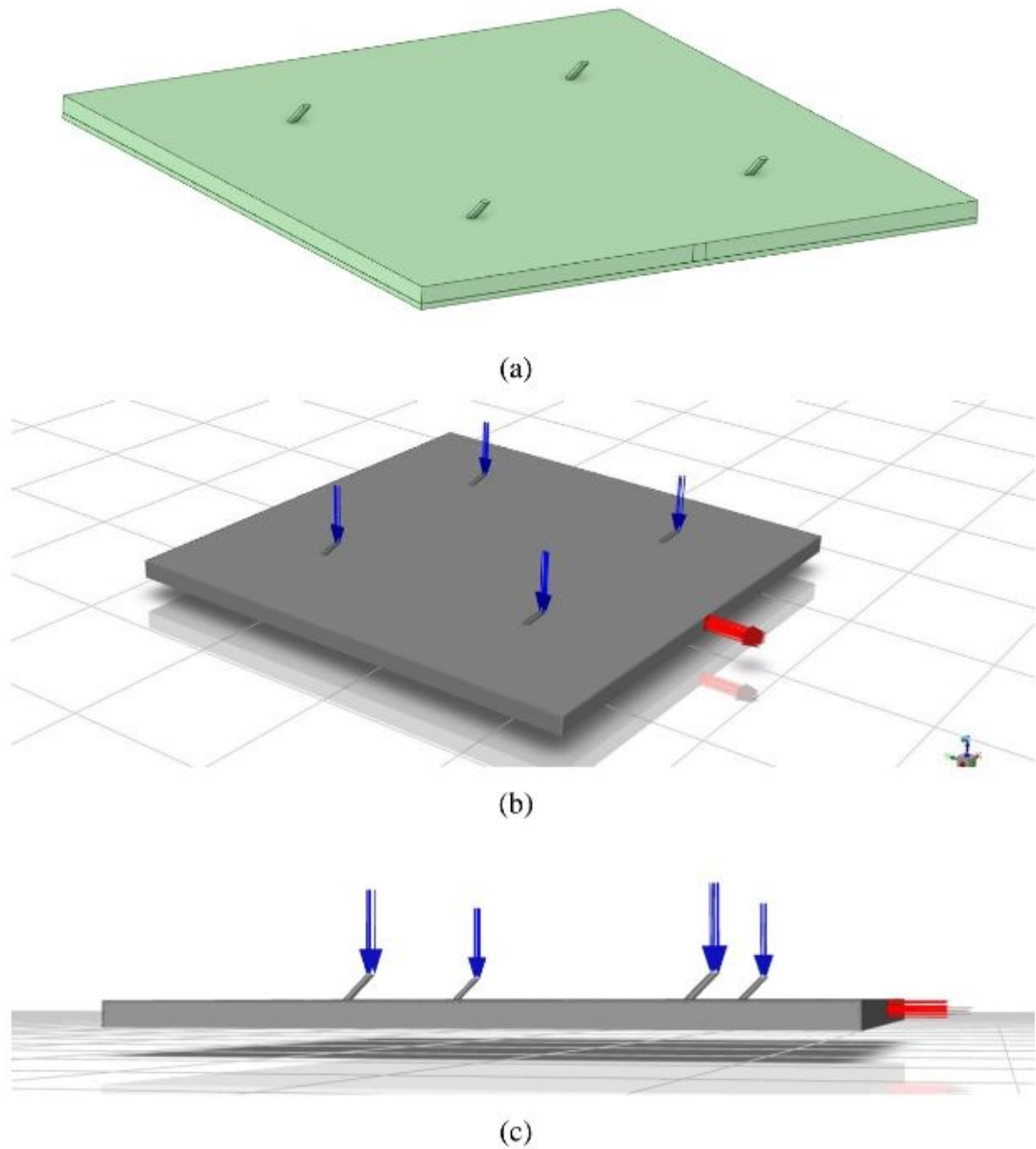


Fig. 3.14: Geometry design of inclined hexagonal 4 micro-jets, E80 (a) Ansys SpaceClaim Geometry (b) Geometry indicating inlets & outlet (c) Side view of geometry indicating inlets & outlet

Table 3.13: Mesh information for E80 hexagonal 4 jets heat sink

Physics solved by	CFD
Solver used	Fluent
Element order	Linear
Curvature Proximity	On
Smoothing	Medium
Element size	5.e-005 m
Nodes	775851
Elements	2036842

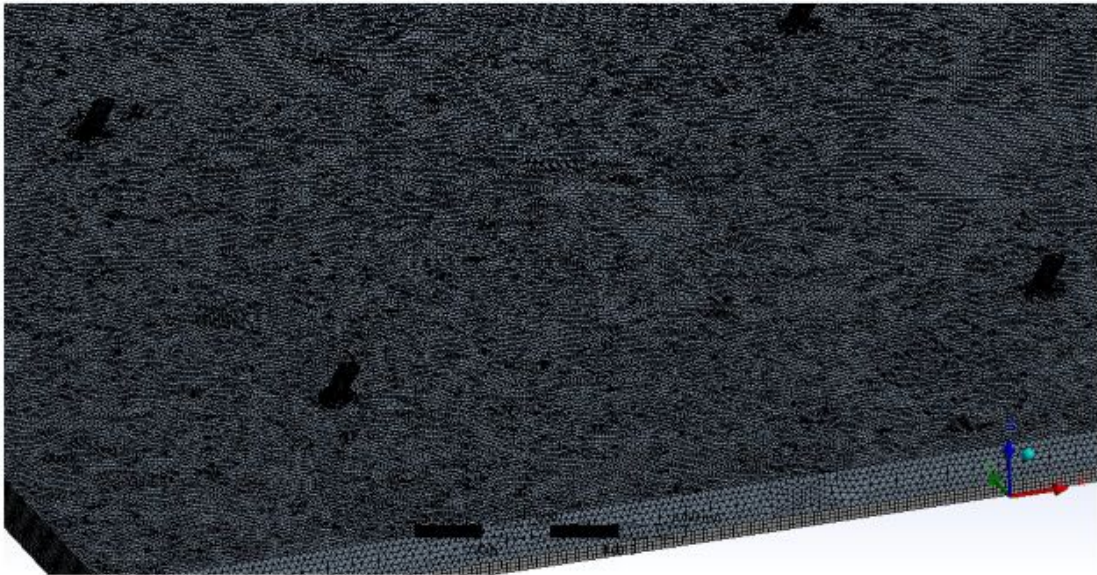


Fig. 3.15 Meshing of inclined hexagonal 4 hex-jet heat sink, E80

Geometry 7 is considered for simulation which is 45° inclined 5 hexagonal cross-section jets of edge length 80 microns. Table 3.14 shows the dimensions parameters of the 5 hex-jets model. Fig. 3.16 presents different views of the geometry showing inlets and outlet. Table 3.15 provides the mesh information considered for simulation. Fig. 3.17 represents the meshing of the 5 hex-jets E80 model.

Geometry 7: 45° inclined 5 micro-jets, E80

Table 3.14: Dimensions for E80 hexagonal 5 jets heat sink

A_{cs} (mm ²)	T_s (μ m)	H_c (μ m)	E (μ m)	H_n (μ m)	S_n (μ m)
11×11	100	300	60	40	2750

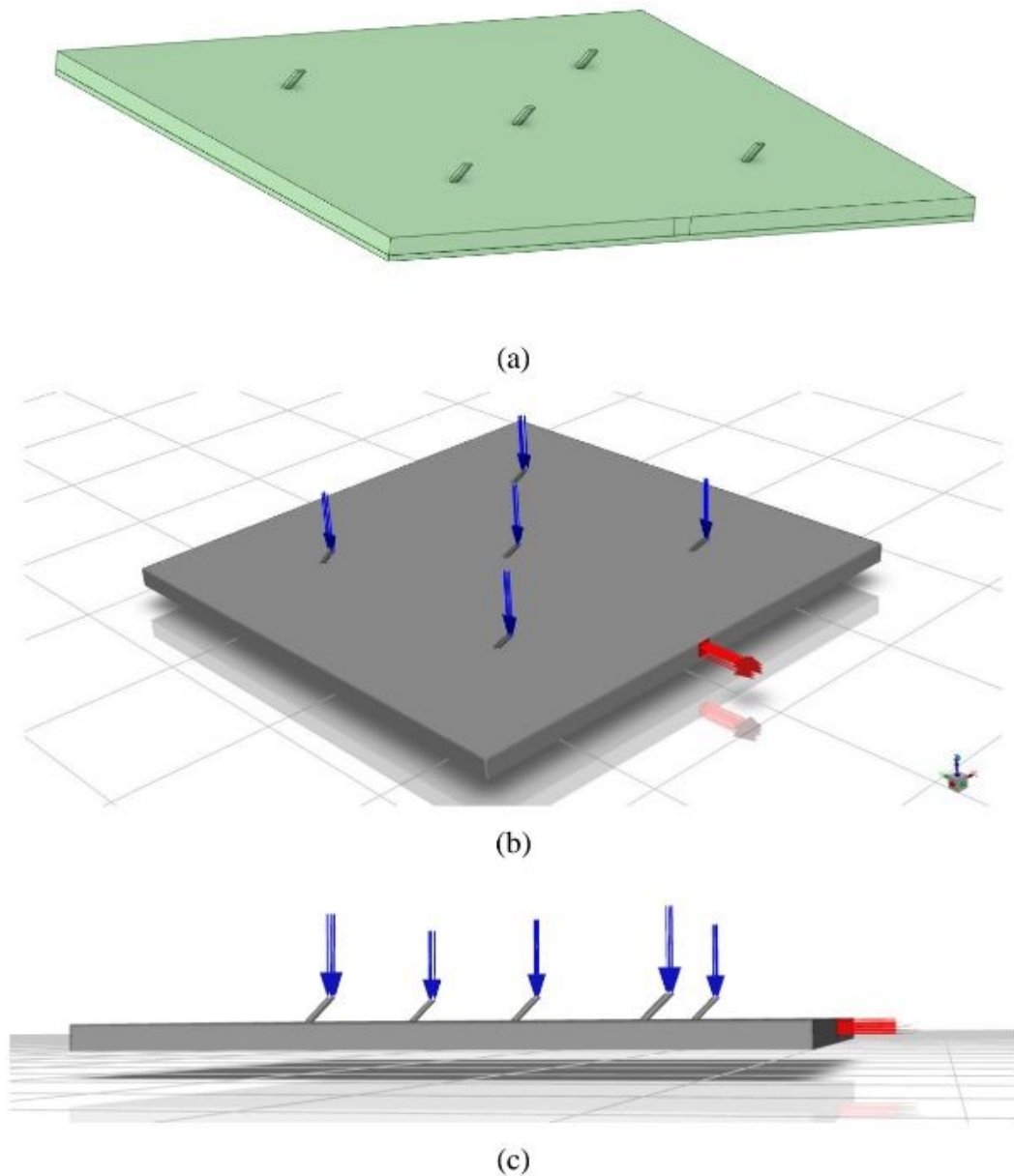


Fig. 3.16: Geometry design of inclined 5 hex-jets heat sink, E80 (a) Ansys SpaceClaim Geometry (b) Geometry indicating inlets & outlet (c) Side view of geometry indicating inlets & outlet

Table 3.15: Mesh information for E80 hexagonal 5 jets heat sink

Physics solved by	CFD
Solver used	Fluent
Element order	Linear
Curvature Proximity	On
Smoothing	Medium
Element size	5.e-005 m
Nodes	775700
Elements	2040228



Fig. 3.17 Meshing of inclined hexagonal 5 hex-jets heat sink, E80

Geometry 8 is considered for simulation which is 45° inclined 9 hexagonal cross-section jets of edge length 80 microns. Table 3.16 shows the dimensions parameters of the 9 hex-jets model. Fig. 3.18 presents different views of the geometry showing inlets and outlet. Table 3.17 provides the mesh information considered for simulation. Fig. 3.19 represents the meshing of the 9 hex-jets E80 model.

Geometry 8 : 45° inclined 9 micro-jets, E80

Table 3.16: Dimensions for E80 hexagonal 9 jets heat sink

A_{cs} (mm ²)	T_s (μ m)	H_c (μ m)	E (μ m)	H_n (μ m)	S_n (μ m)
11×11	100	300	60	40	3750

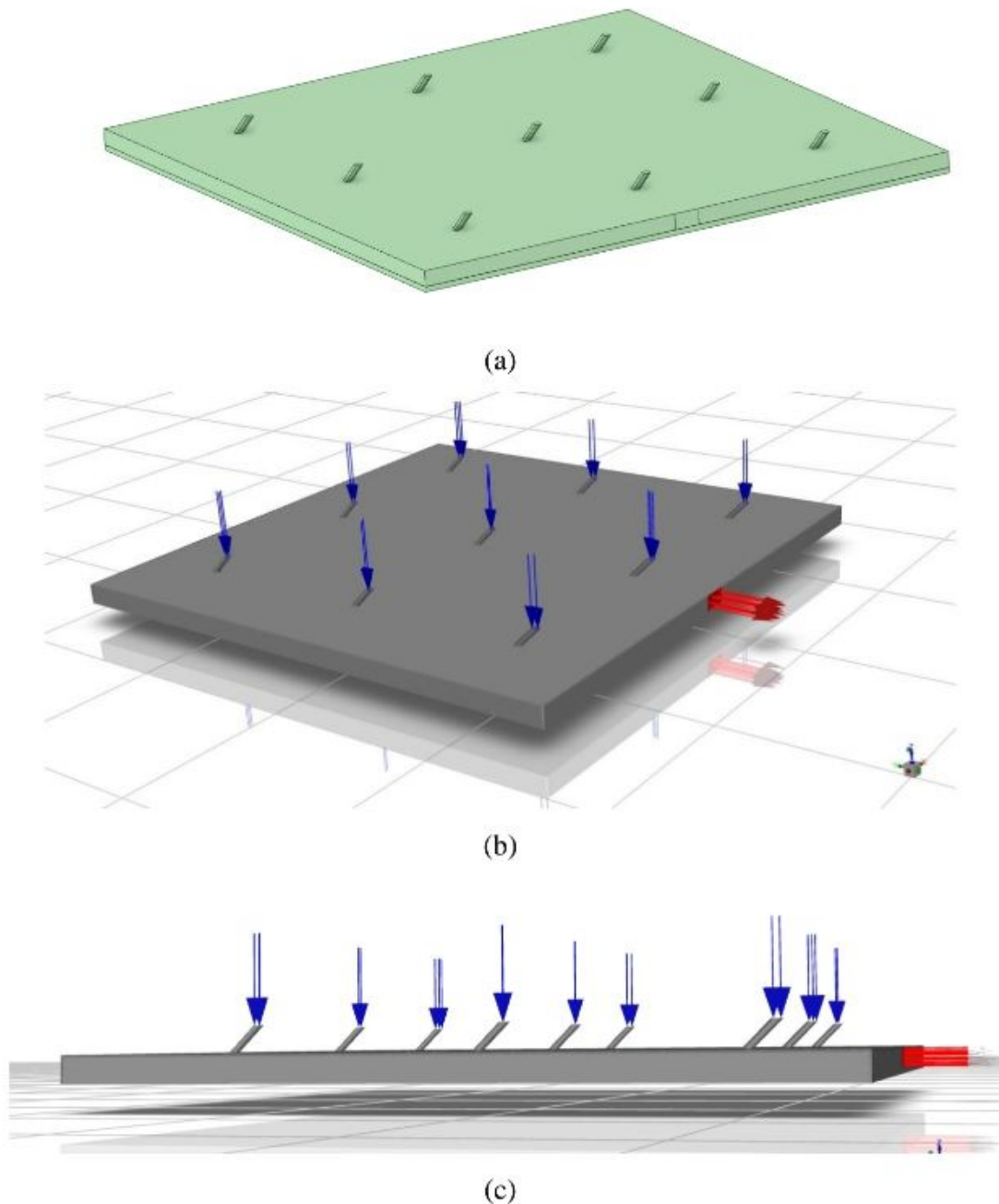


Fig. 3.18: Geometry design of inclined 9 hex-jets heat sink, E80 (a) Ansys SpaceClaim Geometry (b) Geometry indicating inlets & outlet (c) Side view of geometry indicating inlets & outlet

Table 3.17: Mesh information for E80 hexagonal 9 jets heat sink

Physics solved by	CFD
Solver used	Fluent
Element order	Linear
Curvature Proximity	On
Smoothing	Medium
Element size	5.e-005 m
Nodes	778577
Elements	2050544

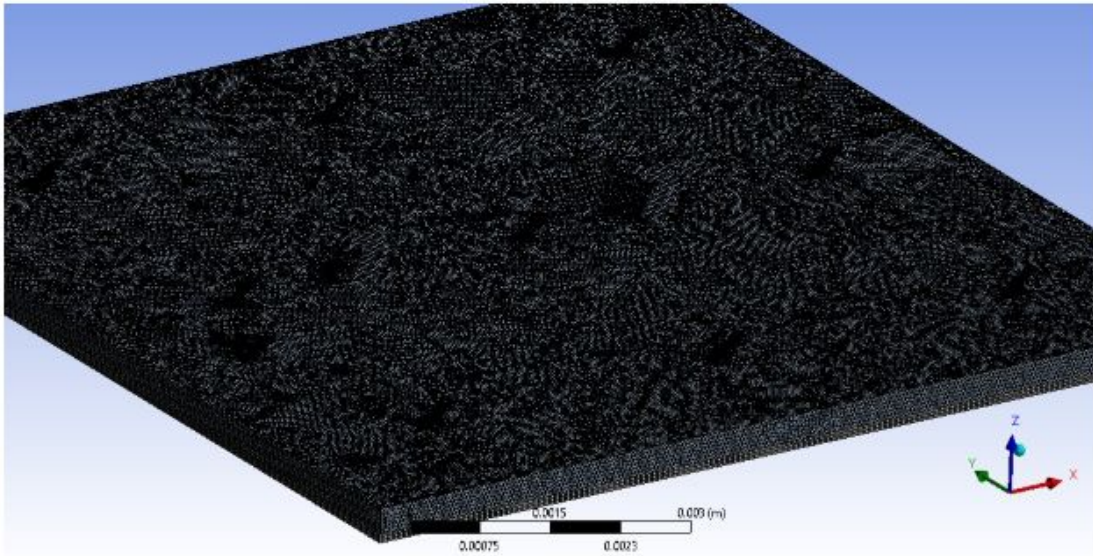


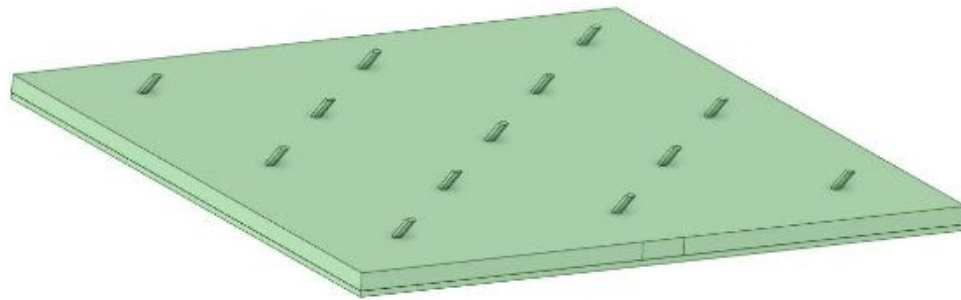
Fig. 3.19 Meshing of inclined hexagonal 9 hex-jet heat sink, E80

Geometry 9 is considered for simulation which is 45° inclined 13 hexagonal cross-section jets of edge length 80 microns. Table 3.18 shows the dimensions parameters of the 13 hex-jets model. Fig. 3.20 presents different views of the geometry showing inlets and outlet. Table 3.19 provides the mesh information considered for simulation. Fig. 3.21 represents the meshing of the 13 hex-jets E80 model.

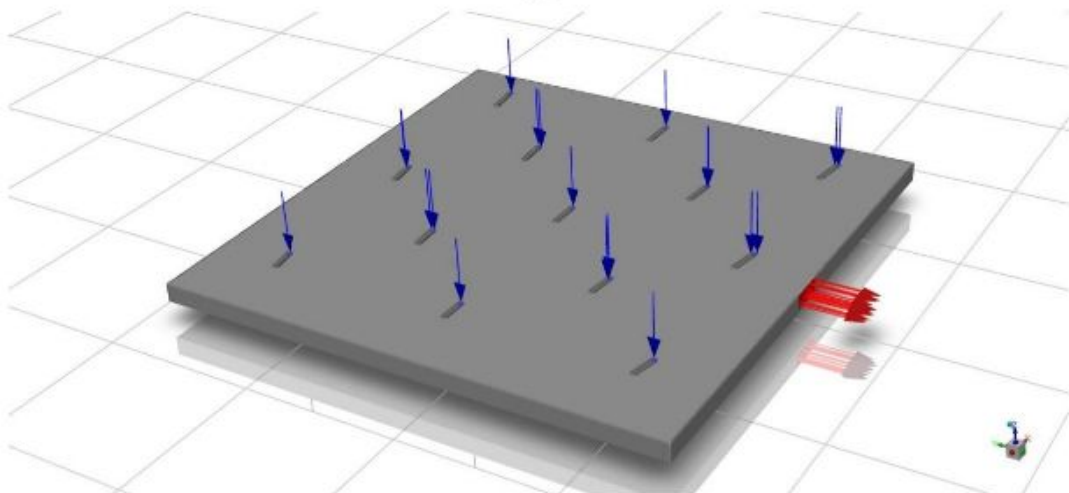
Geometry 9 : 45° inclined 13 micro-jets, E80

Table 3.18: Dimensions for E80 hexagonal 13 jets heat sink

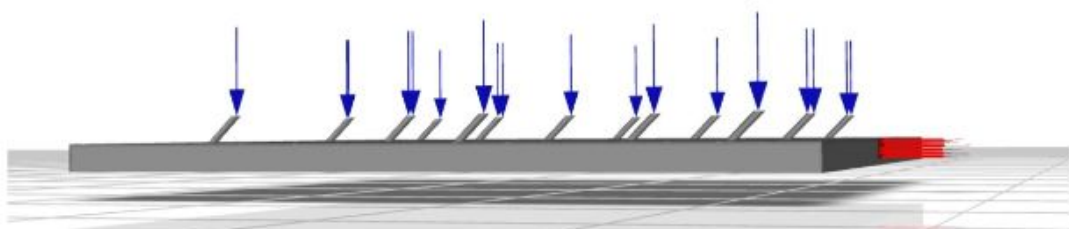
A_{cs} (mm ²)	T_s (μ m)	H_c (μ m)	E (μ m)	H_n (μ m)	S_n (μ m)
11×11	100	300	60	40	2000



(a)



(b)



(c)

Fig. 3.20: Geometry design of inclined 13 hex-jets heat sink, E80 (a) Ansys SpaceClaim Geometry (b) Geometry indicating inlets & outlet (c) Side view of geometry indicating inlets & outlet

Table 3.19: Mesh information for E80 hexagonal 13 jets heat sink

Physics solved by	CFD
Solver used	Fluent
Element order	Linear
Curvature Proximity	On
Smoothing	Medium
Element size	5.e-005 m
Nodes	782921
Elements	2069575

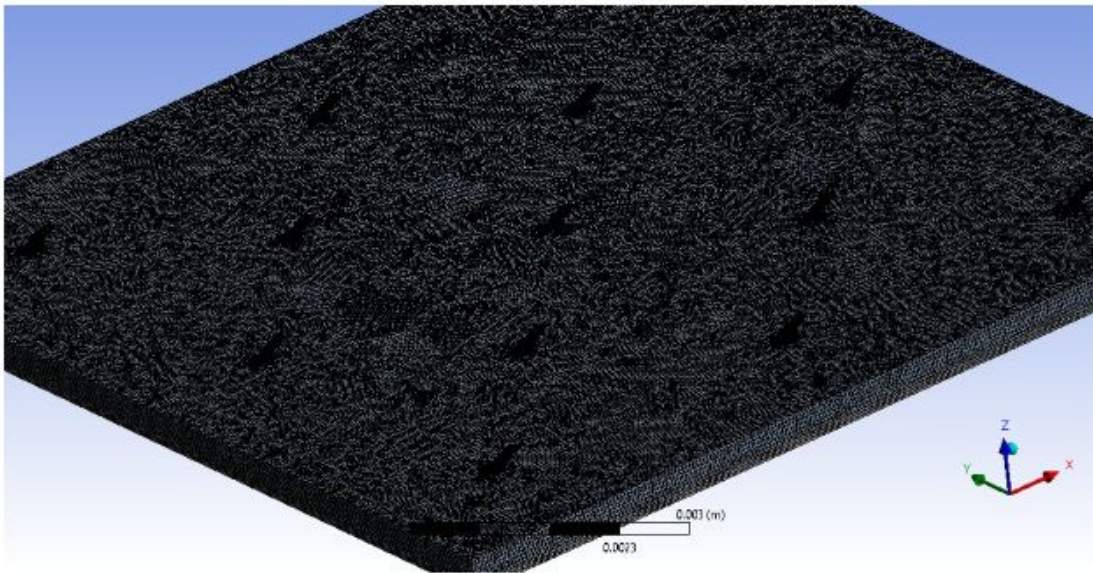


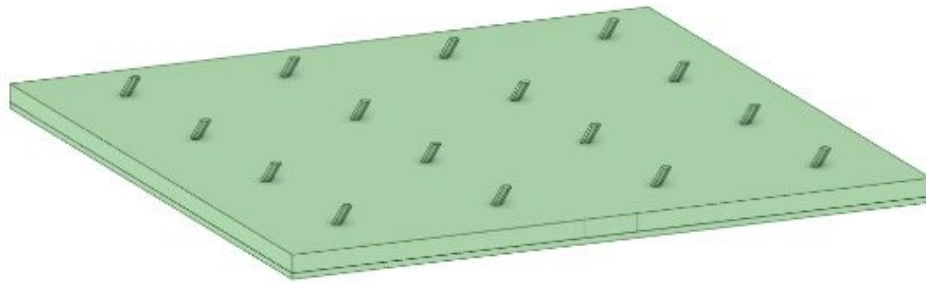
Fig. 3.21 Meshing of inclined hexagonal 13 hex-jet heat sink, E80

Geometry 10 is considered for simulation which is 45° inclined 16 hexagonal cross-section jets of edge length 80 microns. Table 3.20 shows the dimensions parameters of the 16 hex-jets model. Fig. 3.22 presents different views of the geometry showing inlets and outlet. Table 3.21 provides the mesh information considered for simulation. Fig. 3.23 represents the meshing of the 16 hex-jets E80 model.

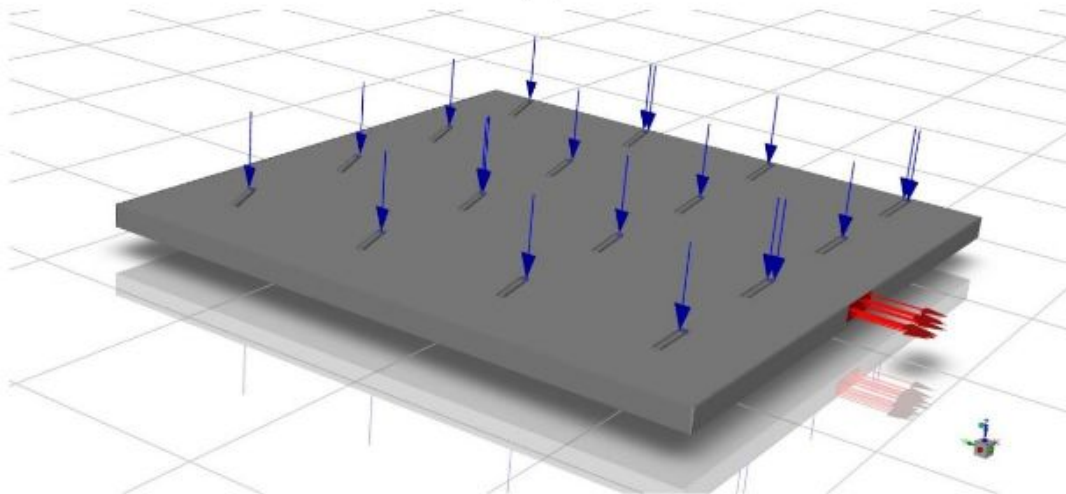
Geometry 10 : 45° inclined 16 micro-jets, E80

Table 3.20: Dimensions for E80 hexagonal 16 jets heat sink

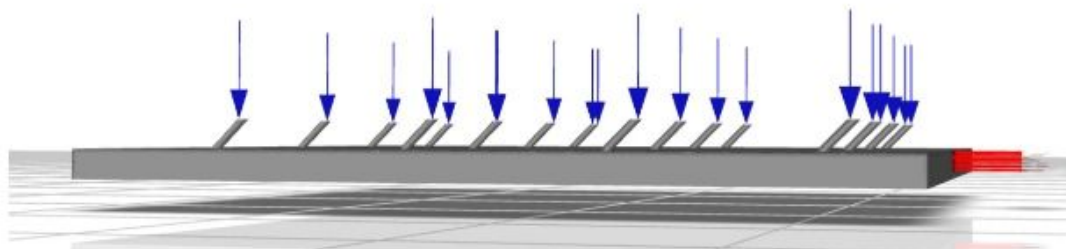
A_{cs} (mm ²)	T_s (μ m)	H_c (μ m)	E (μ m)	H_n (μ m)	S_n (μ m)
11 \times 11	100	300	60	40	2750



(a)



(b)



(c)

Fig. 3.22: Geometry design of inclined 16 hex-jets heat sink, E80 (a) Ansys SpaceClaim Geometry (b) Geometry indicating inlets & outlet (c) Side view of geometry indicating inlets & outlet

Table 3.21: Mesh information for E80 hexagonal 16 jets heat sink

Physics solved by	CFD
Solver used	Fluent
Element order	Linear
Curvature Proximity	On
Smoothing	Medium
Element size	5.e-005 m
Nodes	785714
Elements	2081979

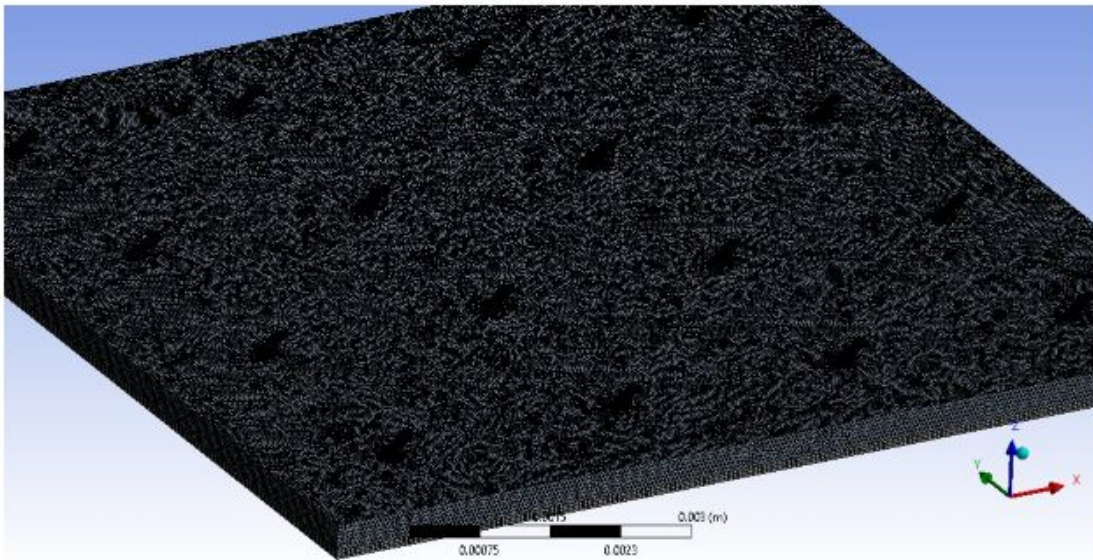


Fig. 3.23 Meshing of inclined hexagonal 16 hex-jet heat sink, E80

Geometry 11 is considered for simulation which is 45° inclined 4 hexagonal cross-section jets of edge length 100 microns. Table 3.22 shows the dimensions parameters of the 4 hex-jets model. Fig. 3.24 presents different views of the geometry showing inlets and outlet. Table 3.23 provides the mesh information considered for simulation. Fig. 3.25 represents the meshing of the 4 hex-jets E100 model.

Geometry 11 : 45° inclined 4 micro-jets, E100

Table 3.22: Dimensions for E100 hexagonal 4 jets heat sink

A_{cs} (mm ²)	T_s (μ m)	H_c (μ m)	E (μ m)	H_n (μ m)	S_n (μ m)
11×11	100	300	60	40	5500

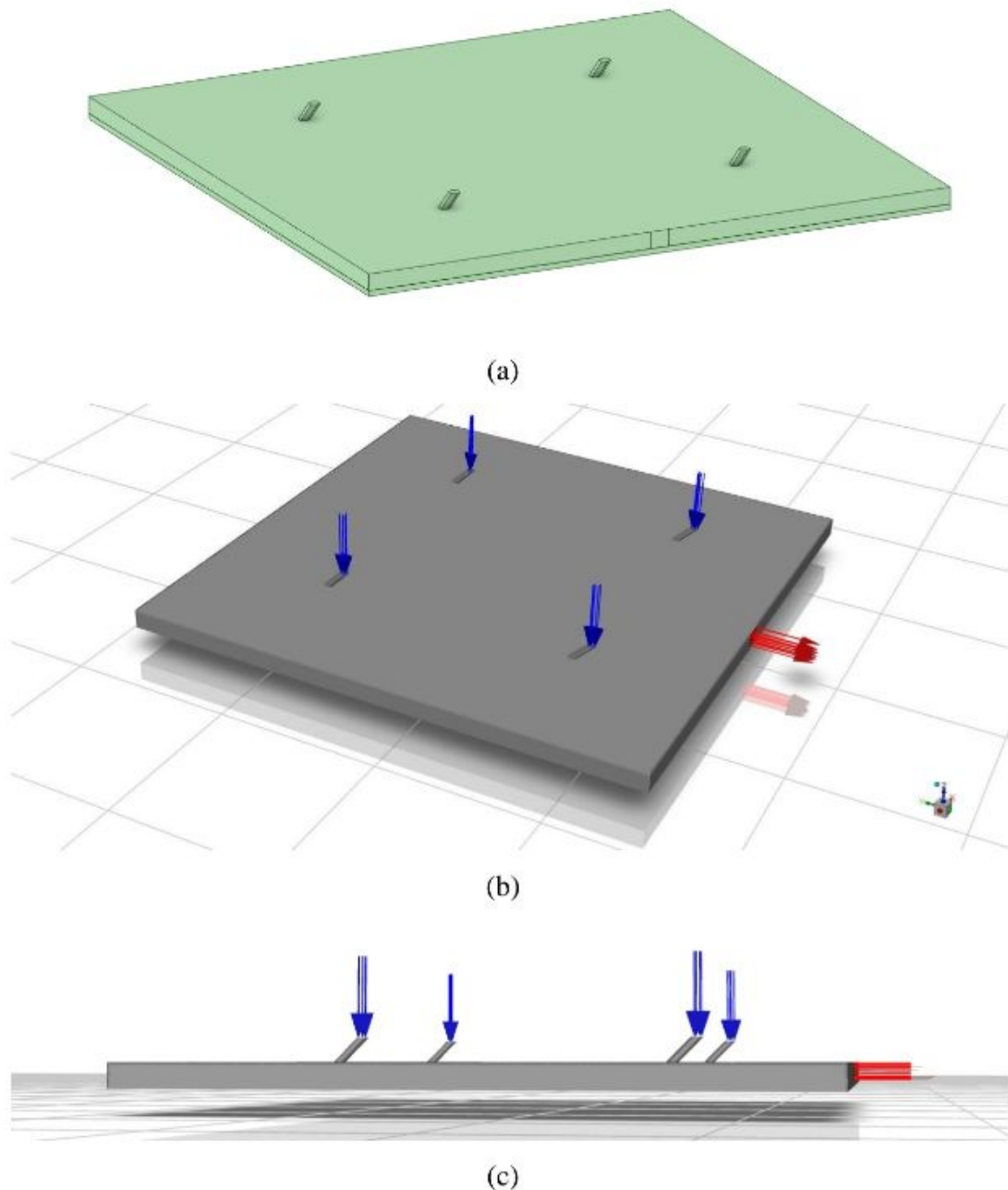


Fig. 3.24: Geometry design of inclined 4 hex-jets heat sink, E100 (a) Ansys SpaceClaim Geometry (b) Geometry indicating inlets & outlet (c) Side view of geometry indicating inlets & outlet

Table 3.23: Mesh information for E100 hexagonal 4 jets heat sink

Physics solved by	CFD
Solver used	Fluent
Element order	Linear
Curvature Proximity	On
Smoothing	Medium
Element size	5.e-005 m
Nodes	772723
Elements	2027438

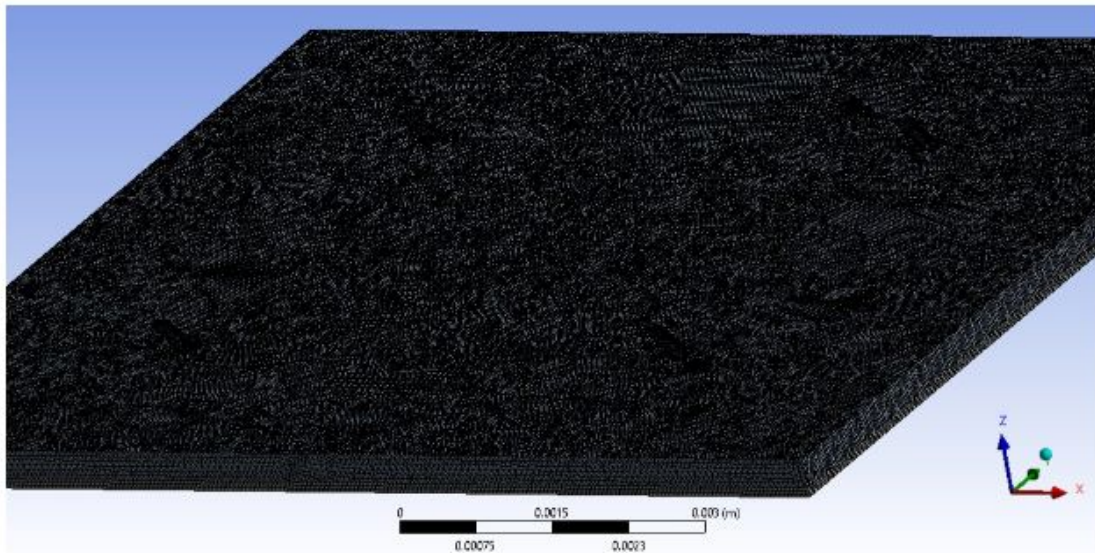


Fig. 3.25: Meshing of inclined hexagonal 4 hex-jet heat sink, E100

Geometry 12 is considered for simulation which is 45° inclined 5 hexagonal cross-section jets of edge length 100 microns. Table 3.24 shows the dimensions parameters of the 5 hex-jets model. Fig. 3.26 presents different views of the geometry showing inlets and outlet. Table 3.25 provides the mesh information considered for simulation. Fig. 3.27 represents the meshing of the 5 hex-jets E100 model.

Geometry 12 : 45° inclined 5 micro-jets, E100

Table 3.24: Dimensions for E100 hexagonal 5 jets heat sink

A_{cs} (mm ²)	T_s (μ m)	H_c (μ m)	E (μ m)	H_n (μ m)	S_n (μ m)
11×11	100	300	60	40	2750

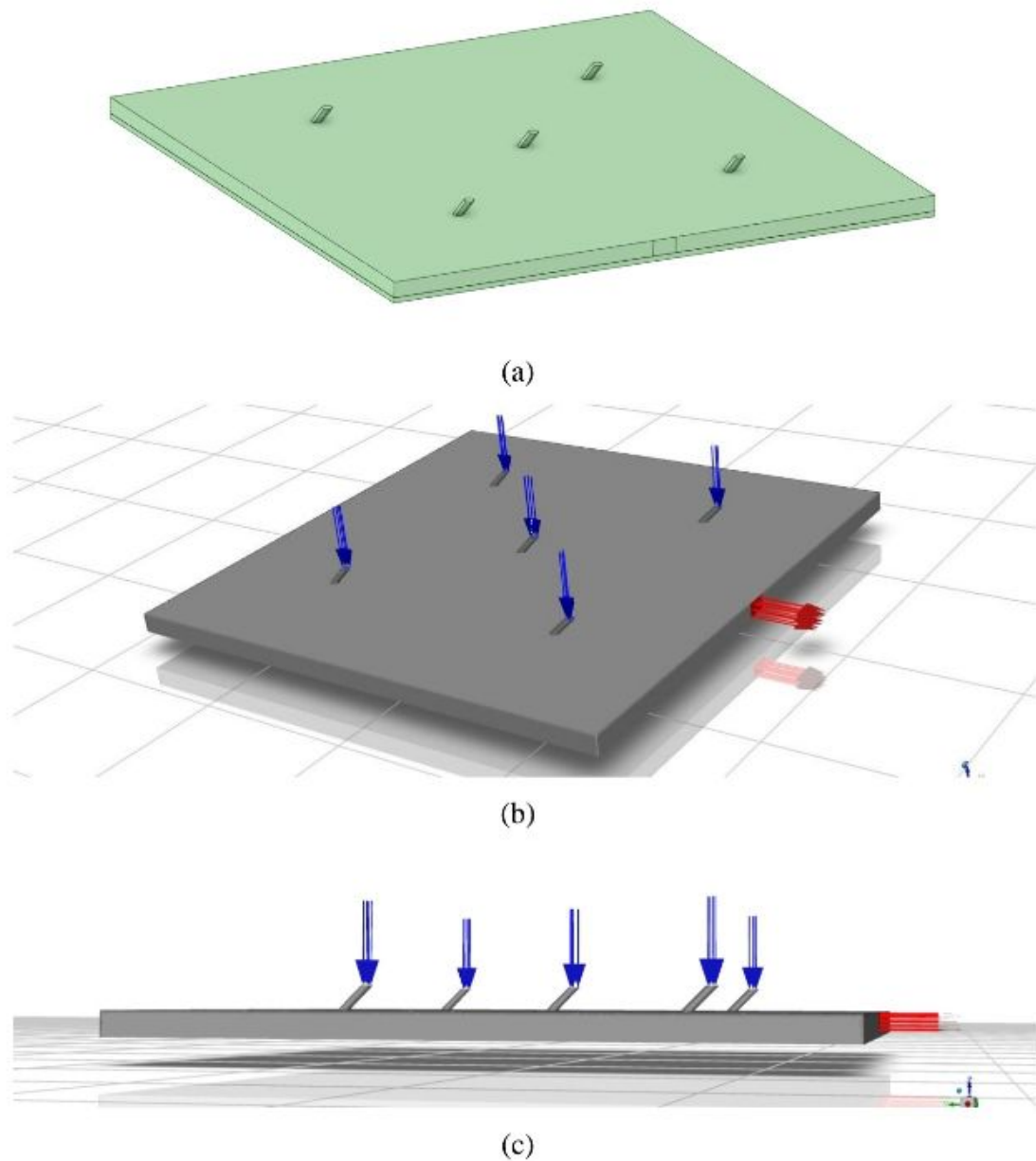


Fig. 3.26. Geometry design of inclined 5 hex-jets heat sink, E100 (a) Ansys SpaceClaim Geometry (b) Geometry indicating inlets & outlet (c) Side view of geometry indicating inlets & outlet

Table 3.25. Mesh information for E100 hexagonal 5 jets heat sink

Physics solved by	CFD
Solver used	Fluent
Element order	Linear
Curvature Proximity	On
Smoothing	Medium
Element size	5.e-005 m
Nodes	773700
Elements	2032056

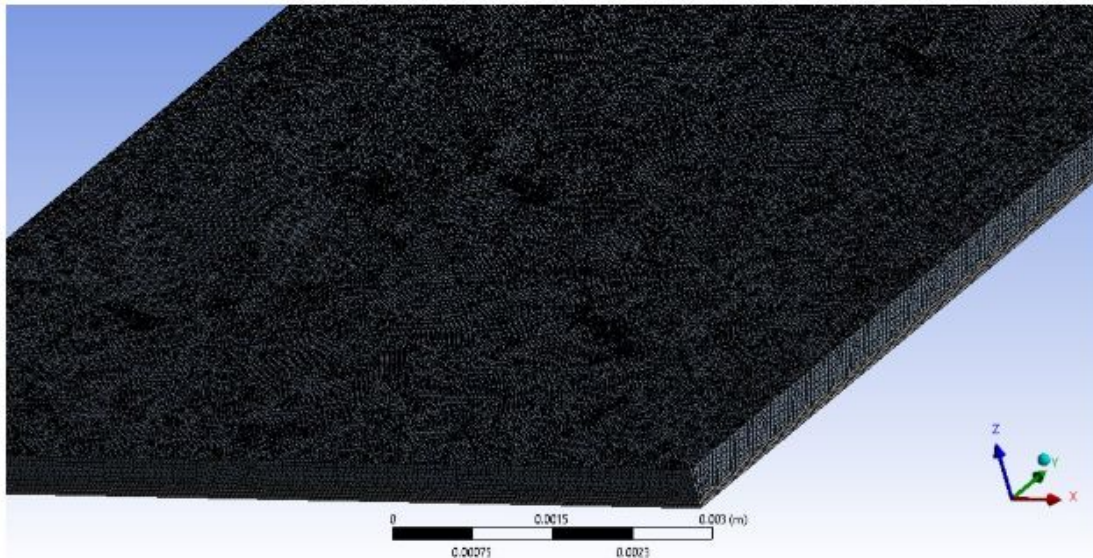


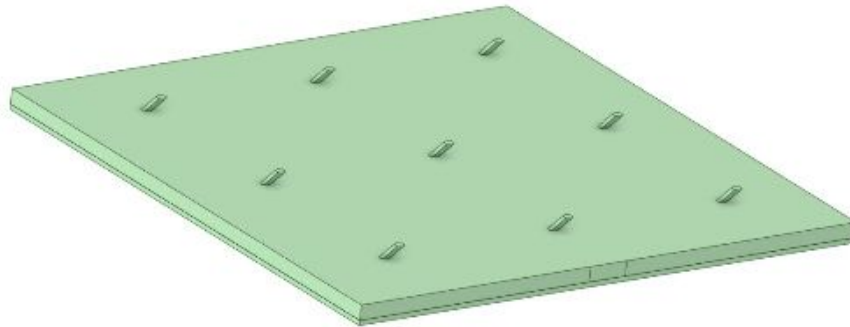
Fig. 3.27. Meshing of inclined hexagonal 5 hex-jet heat sink, E100

Geometry 13 is considered for simulation which is 45° inclined 9 hexagonal cross-section jets of edge length 100 microns. Table 3.26 shows the dimensions parameters of the 9 hex-jets model. Fig. 3.28 presents different views of the geometry showing inlets and outlet. Table 3.27 provides the mesh information considered for simulation. Fig. 3.29 represents the meshing of the 9 hex-jets E100 model.

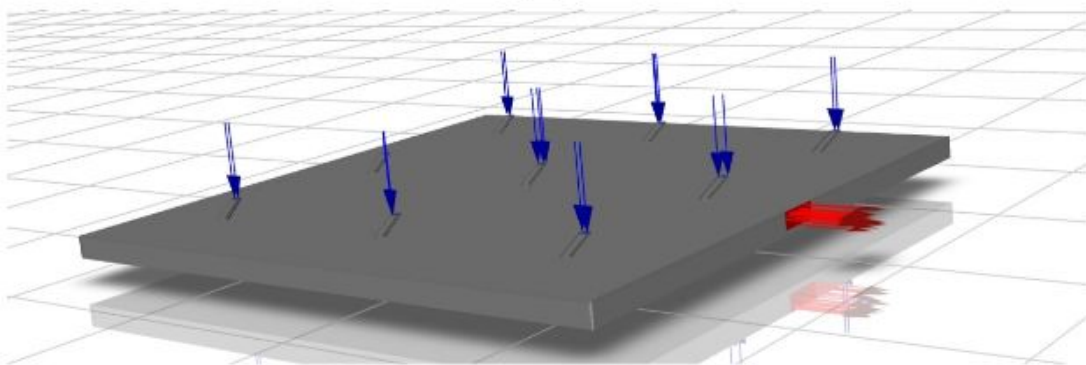
Geometry 13 : 45° inclined 9 micro-jets, E100

Table 3.26: Dimensions for E100 hexagonal 9 jets heat sink

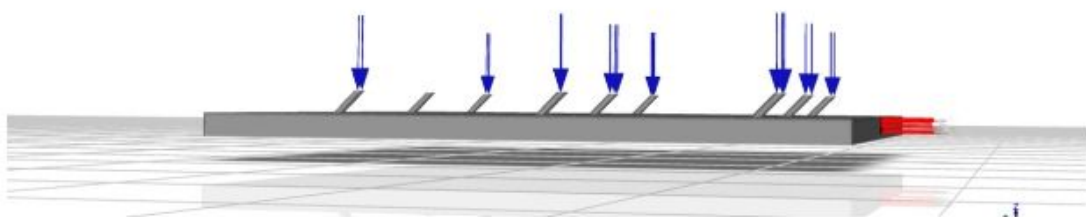
A_{cs} (mm ²)	T_s (μ m)	H_c (μ m)	E (μ m)	H_n (μ m)	S_n (μ m)
11×11	100	300	60	40	3750



(a)



(b)



(c)

Fig. 3.28. Geometry design of inclined 9 hex-jets heat sink, E100 (a) Ansys SpaceClaim Geometry (b) Geometry indicating inlets & outlet (c) Side view of geometry indicating inlets & outlet

Table 3.27: Mesh information for E100 hexagonal 9 jets heat sink

Physics solved by	CFD
Solver used	Fluent
Element order	Linear
Curvature Proximity	On
Smoothing	Medium
Element size	5.e-005 m
Nodes	775317
Elements	2035037

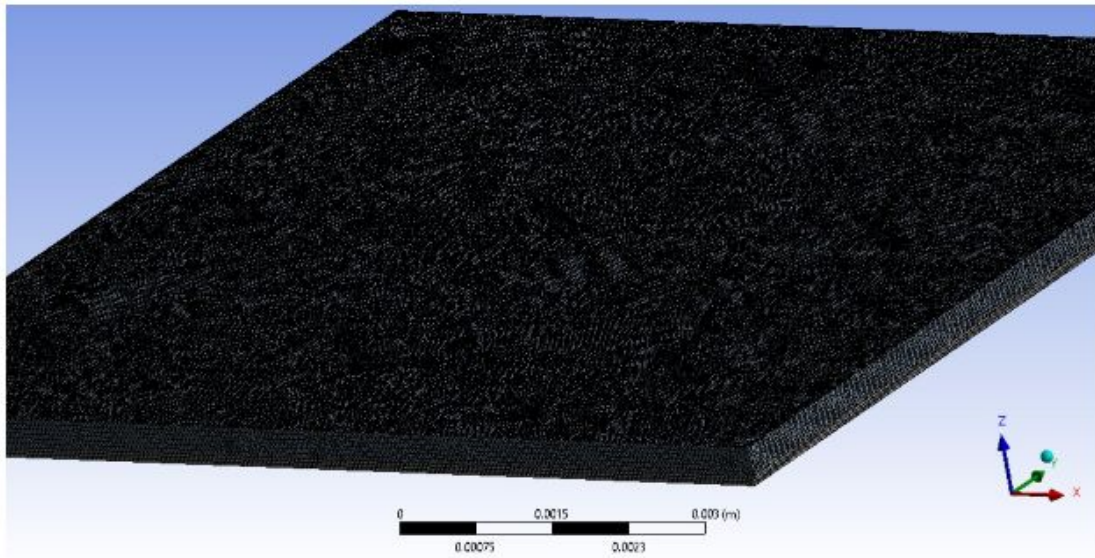


Fig. 3.29 Meshing of inclined hexagonal 9 hex-jet heat sink, E100

Geometry 14 is considered for simulation which is 45° inclined 13 hexagonal cross-section jets of edge length 100 microns. Table 3.28 shows the dimensions parameters of the 13 hex-jets model. Fig. 3.30 presents different views of the geometry showing inlets and outlet. Table 3.29 provides the mesh information considered for simulation. Fig. 3.31 represents the meshing of the 13 hex-jets E100 model.

Geometry 14 : 45° inclined 13 micro-jets, E100

Table 3.28: Dimensions for E100 hexagonal 13 jets heat sink

A_{cs} (mm ²)	T_s (μ m)	H_c (μ m)	E (μ m)	H_n (μ m)	S_n (μ m)
11 \times 11	100	300	60	40	2000

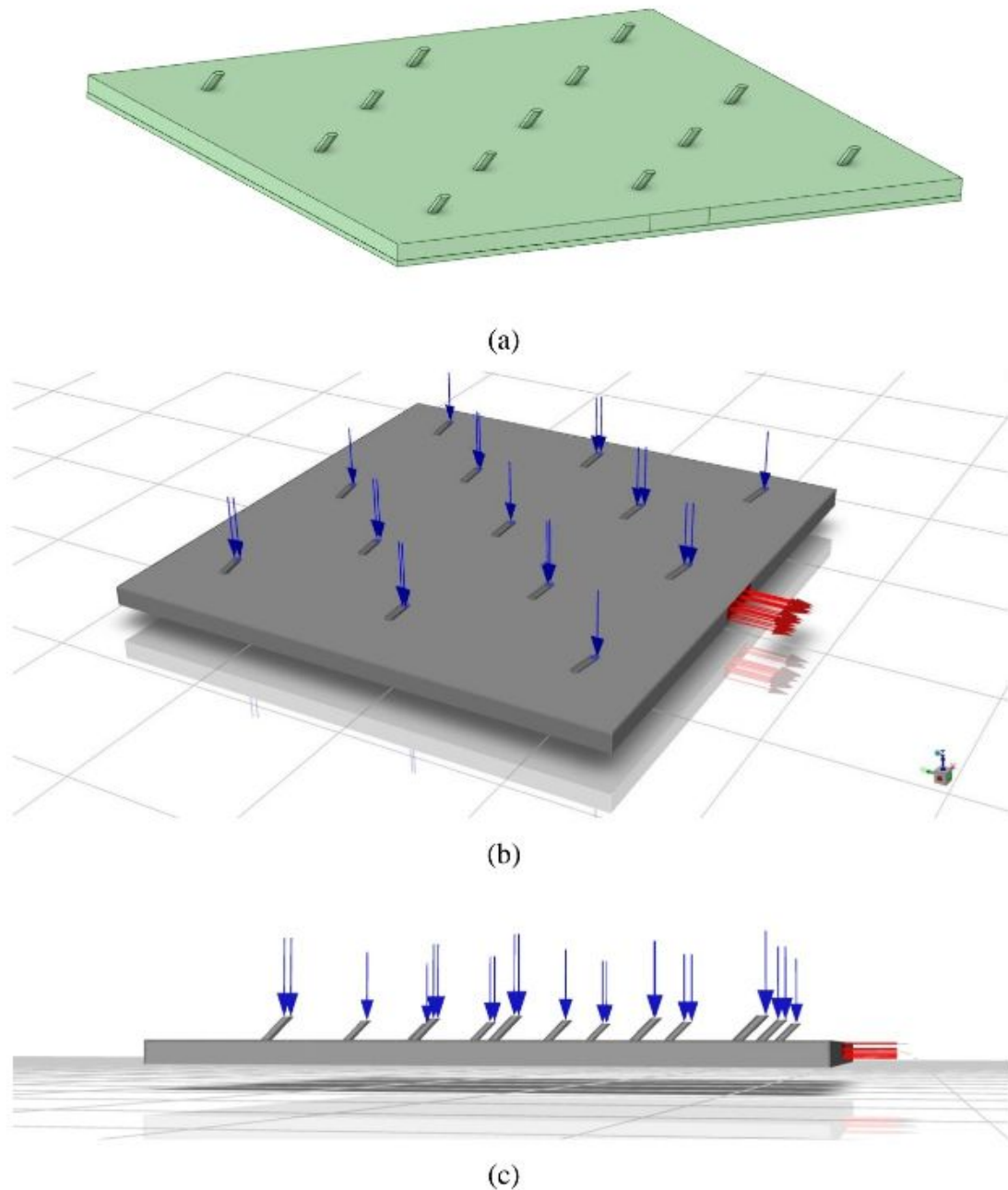


Fig. 3.30. Geometry design of inclined 13 hex-jets heat sink, E100 (a) Ansys SpaceClaim Geometry (b) Geometry indicating inlets & outlet (c) Side view of geometry indicating inlets & outlet

Table 3.29: Mesh information for E100 hexagonal 13 jets heat sink

Physics solved by	CFD
Solver used	Fluent
Element order	Linear
Curvature Proximity	On
Smoothing	Medium
Element size	5.e-005 m
Nodes	778330
Elements	2047759



Fig. 3.31 Meshing of inclined hexagonal 13 hex-jet heat sink, E100

Geometry 15 is considered for simulation which is 45° inclined 16 hexagonal cross-section jets of edge length 100 microns. Table 3.30 shows the dimensions parameters of the 16 hex-jets model. Fig. 3.32 presents different views of the geometry showing inlets and outlet. Table 3.31 provides the mesh information considered for simulation. Fig. 3.33 represents the meshing of the 16 hex-jets E100 model.

Geometry 15 : 45° inclined 16 micro-jets, E100

Table 3.30: Dimensions for E100 hexagonal 16 jets heat sink

A_{cs} (mm ²)	T_s (μ m)	H_c (μ m)	E (μ m)	H_n (μ m)	S_n (μ m)
11×11	100	300	60	40	2750

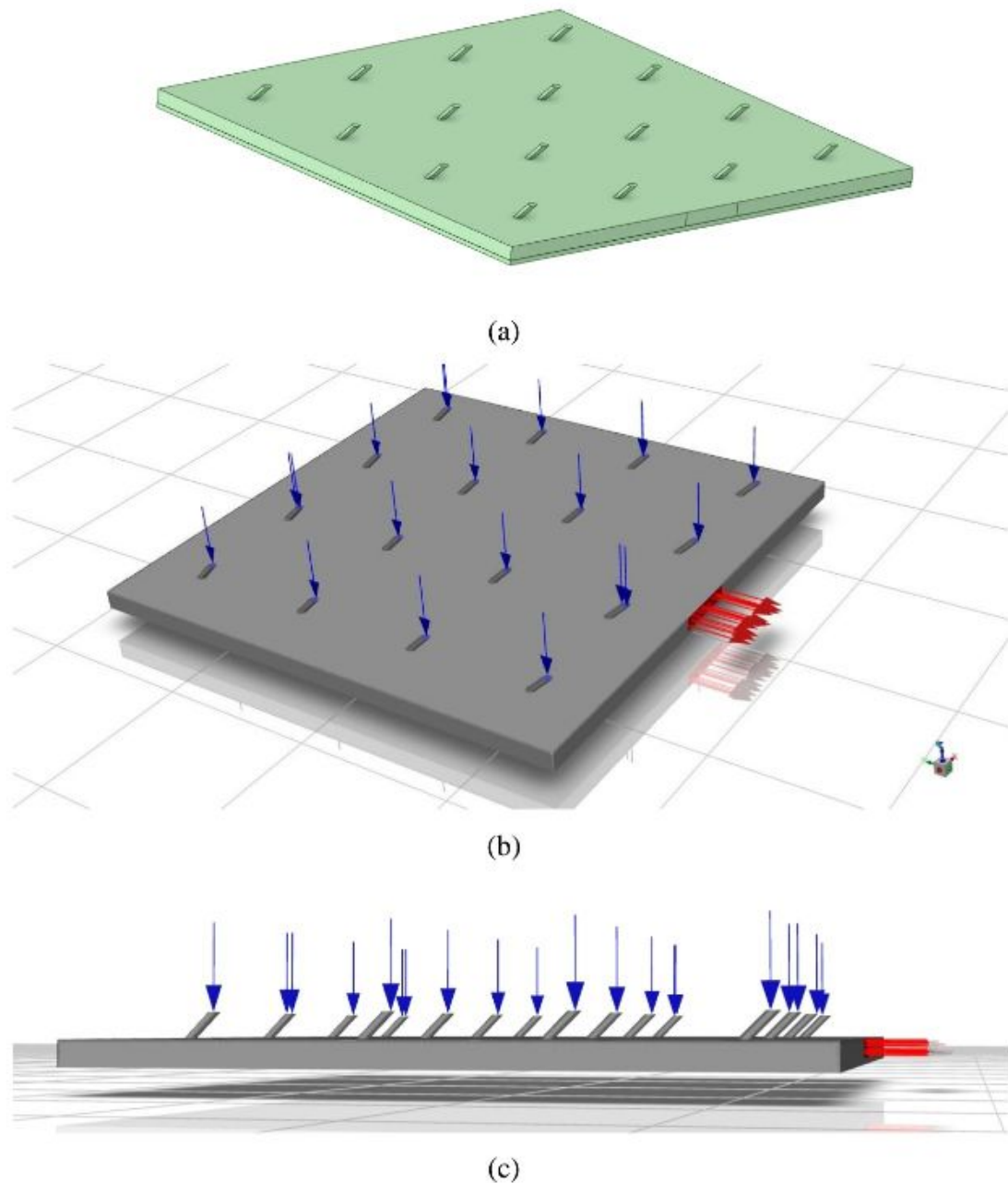


Fig. 3.32. Geometry design of inclined 16 hex-jets heat sink, E100 (a) Ansys SpaceClaim Geometry (b) Geometry indicating inlets & outlet (c) Side view of geometry indicating inlets & outlet

Table 3.31: Mesh information for E100 hexagonal 16 jets heat sink

Physics solved by	CFD
Solver used	Fluent
Element order	Linear
Curvature Proximity	On
Smoothing	Medium
Element size	5.e-005 m
Nodes	779750
Elements	2052346

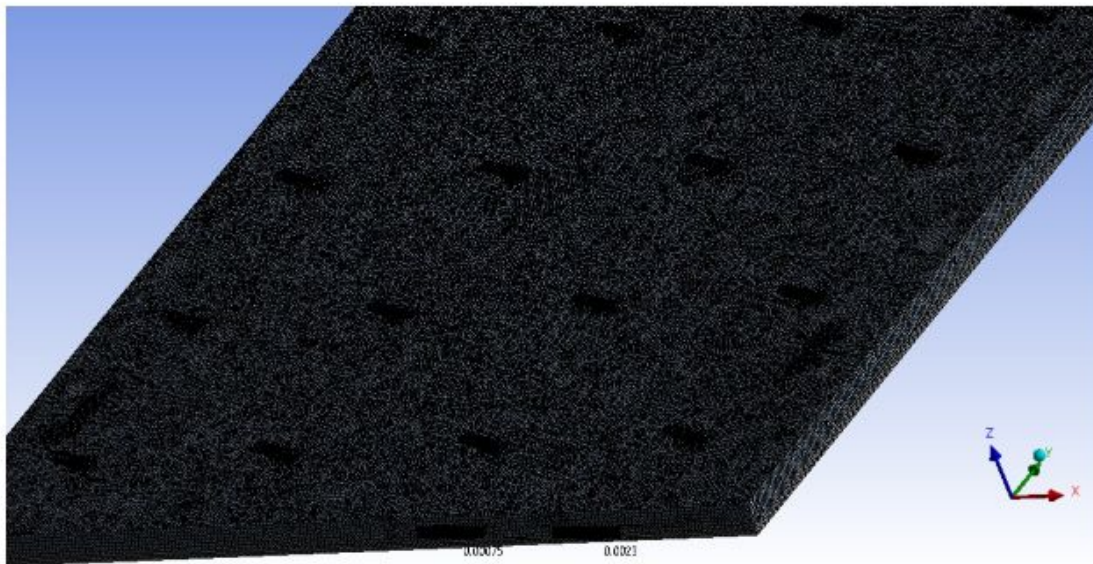


Fig. 3.33 Meshing of inclined hexagonal 16 hex-jet heat sink, E100

CHAPTER 4:

VALIDATION AND GRID INDEPENDENCE TEST

4.1 VALIDATION

The validation part of the thesis focuses on evaluating and verifying the results in relation to the maximum temperature rise in the MCHS with various mass flow rates. The purpose of this section is to confirm the validity of the research's findings in terms of correctness and dependability. Examining the liquid channel - solid substrate contact zone and comparing the simulated results with existing literature are both steps in the validation process that verify the reliability and integrity of the results.

In this computational study, the validation of the staggered 13 vertical straight jets MCHS heat transport by water liquid is conducted. For comparison with the real results, the obtained results are then used to construct graphs that indicate the maximum temperature differential rise with different mass flow rates as shown in Fig. 4.1.1.

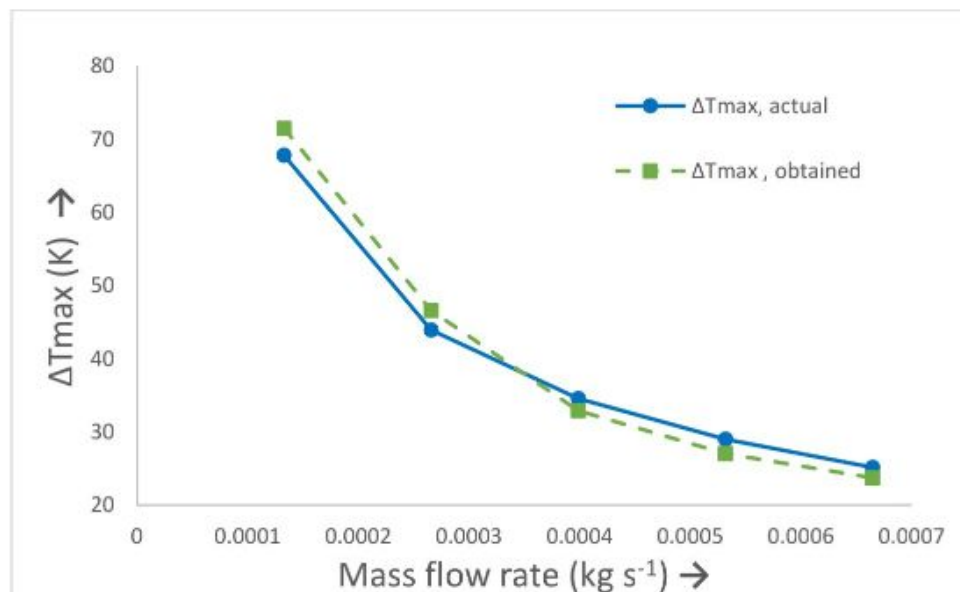


Fig. 4.1.1 Variation ΔT_{\max} , actual & ΔT_{\max} , obtained with mass flow rate

Table 4.1.1 presents the variation in the maximum temperature difference between the actual and obtained results of the fluid-solid interface temp. as mass flow rate increases, calculating the percentage inaccuracy.

Table 4.1.1: Variation ΔT_{\max} , actual & ΔT_{\max} , obtained with mass flow rate to calculate % Error

S. No.	Mass Flow Rate, (kg s^{-1})	ΔT_{\max} , actual (K)	ΔT_{\max} , obtained (K)	% Error
1	1.33×10^{-4}	67.77	71.48	5.47 %
2	2.66×10^{-4}	43.93	46.56	5.98%
3	3.99×10^{-4}	34.55	32.88	4.83%
4	5.32×10^{-4}	28.98	27.62	5.73%
5	6.65×10^{-4}	25.15	23.72	5.68%

As a result, validation of the computational results acquired using test data or existing distributed investigation data is necessary. The results of this investigation were accepted based on the real results of the inquiry, where the maximum error within the result was discovered to be 5.98% and the smallest error was found to be 4.83%.

4.2 GRID INDEPENDENCE TEST

Testing for grid independence is done to determine how sensitive the CFD findings are to changes in the computational grid's resolution or level of refinement. So, to find the optimum no. mesh 4 hexagonal micro jet model is selected. To evaluate this grid sensitivity analysis various mesh size is considered and to find the minimum average temperature of surface of silicon based solid substrate which is solid – liquid interface. Initially, analysis started with taking 5 lakhs mesh and then followed by 10 lakhs, 15 lakhs, 20 lakhs and 30 lakhs mesh size was evaluated.

Model selected for grid analysis: 4 hexagonal jets model

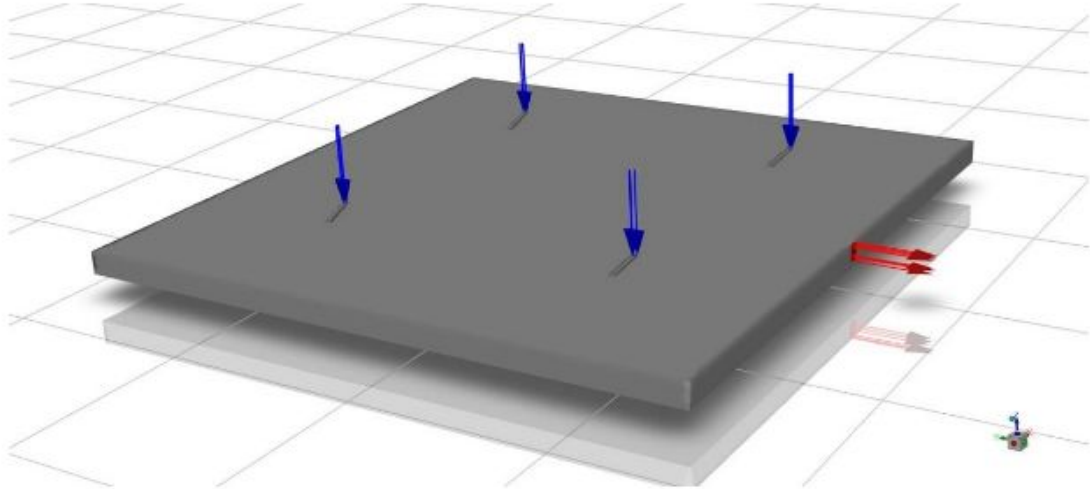


Fig. 4.2.1 Four hexagonal jets model showing inlet and outlet

Table 4.2.1: Avg. Temp. of solid & liquid interface with respect to mesh size

Mesh Size	Avg. Temp. solid & liquid interface
541517	470.231
953601	467.043
1538491	465.911
2049094	465.846
3170114	465.970

By seeing Fig. 4.2.2. it can be understood that at low no. of mesh of 5 lakhs average temperature of substrate surface is high in comparison with high no. mesh size. With increase in no. of mesh size, T_{avg} decreases which indicates that simulation quality of CFD improves. As we move forward in increasing mesh size, stabilisation of T_{avg} is observed which means there is no significant improvement in simulation result. Here, we're getting optimum mesh size for desired minimum T_{avg} . Therefore, mesh size of 2 million is selected for further CFD simulations in this project.

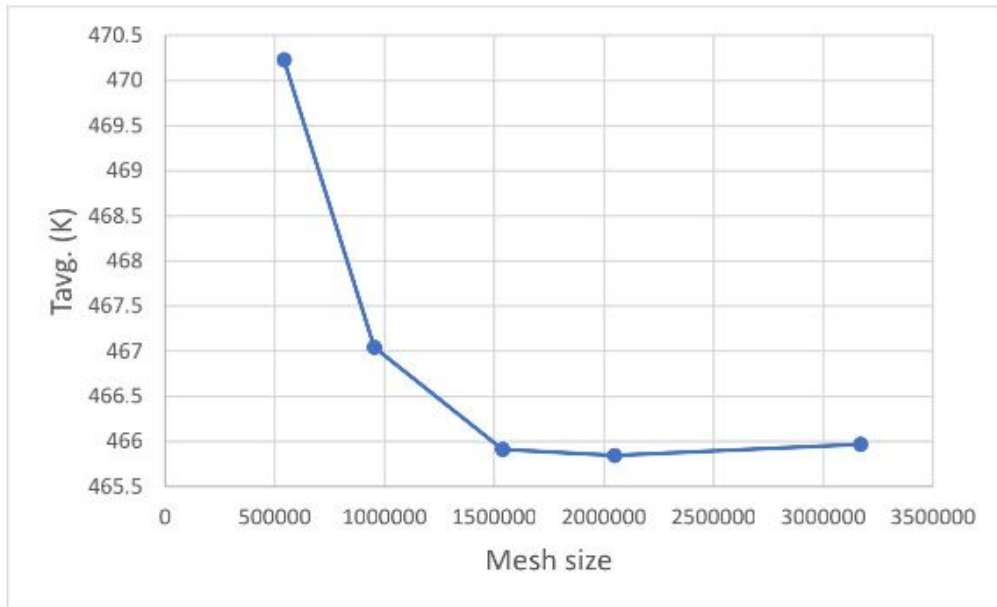


Fig. 4.2.2 Variation of T_{avg} with respect to mesh size selected for simulation

CHAPTER 5:

RESULTS AND DISCUSSION

SIMULATION RESULTS FOR VARIOUS MICRO-JET CONFIGURATIONS IN HEAT SINK

The results of the CFD study are presented for the pressure drop throughout the channel and the temperature drop of the heated surface. These plots are generated for different numbers of impingement jets in a heat sink. The analysis focuses on a specific heat flux value provided at the bottom wall of the heat sink, where the mass flow rate is constant. Heat flow values of 25 W/cm^2 were employed in the analysis. In order to determine the maximum heat transfer rate and maximum temperature rise, the thermal performance of the various jet designs, including inclined four-jet, staggered five-jet, nine-jet, thirteen-jet, and sixteen-jet arrays, was analyzed. Value of constant mass flow rate taken is $1.45 \times 10^{-4} \text{ kg/s}$ for edge lengths of hexagonal cross-section denoted by E60, E80 and E100 which represents 60, 80 and 100 microns respectively. Edge length is considered as design parameter.

5.1 Results for E60 Hexagonal Cross-Section Micro-Jets Impingement Heat Sink for Various No. Of Jets.

Fig. 5.1.1 provides temperature contours at solid-liquid contact region of impingement heat sink for E60 design models of hexagonal cross-section jet nozzle for multiple no. of jets arrangement on liquid channel. The analysis of the temperature contour on the solid heating surface revealed several important findings. Firstly, a noticeable temperature gradient was observed across the surface, indicating variations in heat transfer. Secondly, a cold spot was identified near the end of the nozzle trajectory on the solid surface, possibly indicating an area of high velocity of fluid striking the solid surface. Conversely, hot spots were observed on both corners of the edge near the exit, which could be attributed to the inclination of jets away from the exit. Additionally, regions with high and low temperatures were clearly visible, providing insight into the heat distribution on the solid surface. The average temp. of solid surface reduces with rise in the no. of jets and lowest temp. comes at 13 jets arrangement.

Fig. 5.1.2 represents the temperature contour of liquid channel in impingement heat sink for E60 design models of several no. of jets. The CFD simulation's liquid channel analysis offers insightful information about the system's thermal behaviour. The existence of high and low temperature zones in the temperature distribution indicated varying thermal gradients along the channel. The detection of hotspots and coldspots revealed troublesome regions, such as possible overheating or insufficient cooling. The impact of fluid movement on temperature profiles was further underlined by the investigation. With increase in no. of jets better distribution of fluid flow is observed.

Fig. 5.1.3 shows the velocity contour where streamlines showing the movement of high velocity fluid through jet nozzles to the low velocity fluid in the liquid channel of heat sink. All 5 velocity contours for all 5 configurations of E60 design models are shown for the analysis. The analysis of the streamline velocity contour on the silicon based solid surface in the microchannel revealed important insights into flow patterns and flow uniformity. The contour plot allowed for the identification of distinct flow patterns along the channel. These flow patterns have significant implications for heat transfer, mass transport, and overall fluid dynamics within the microchannel. Additionally, the velocity contour provided an assessment of flow uniformity, indicating whether the velocity distribution along the solid surface was consistent or exhibited variations. A uniform velocity contour suggests a smooth and consistent flow, which is desirable for applications requiring precise fluid delivery.

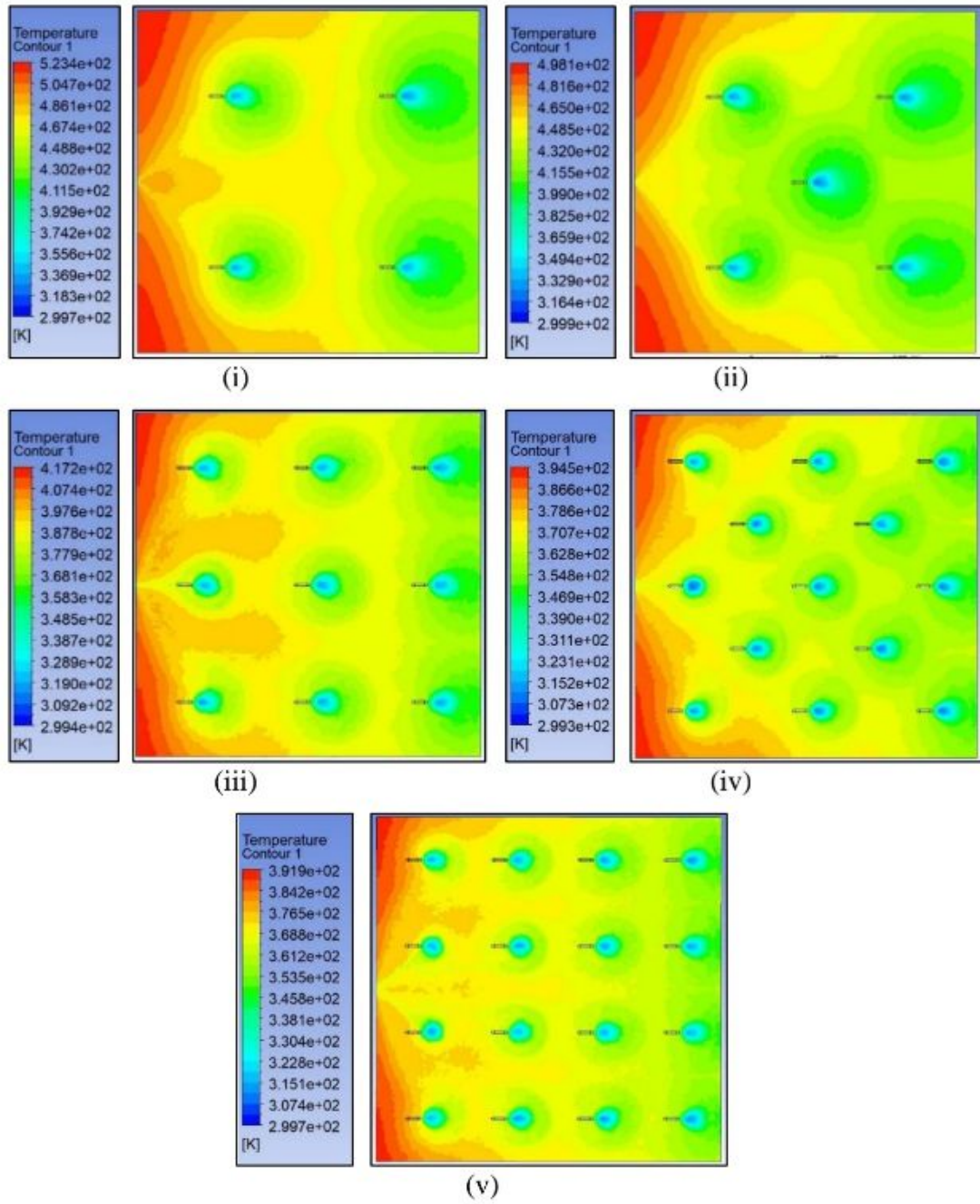


Fig. 5.1.1. Temp. Contours at Solid-Liquid Contact Region for E60 Hexagonal Jets
 (i) 4 hex-jets, (ii) 5 hex-jets, (iii) 9 hex-jets, (iv) 13 hex-jets, (v) 16 hex-jets

Table 5.1.1: T_{avg} of contact region of fluid and solid for E60 design

No. of Jets	Avg. temp. of contact region
4	465.846
5	440.331
9	389.345
13	369.685
16	370.323

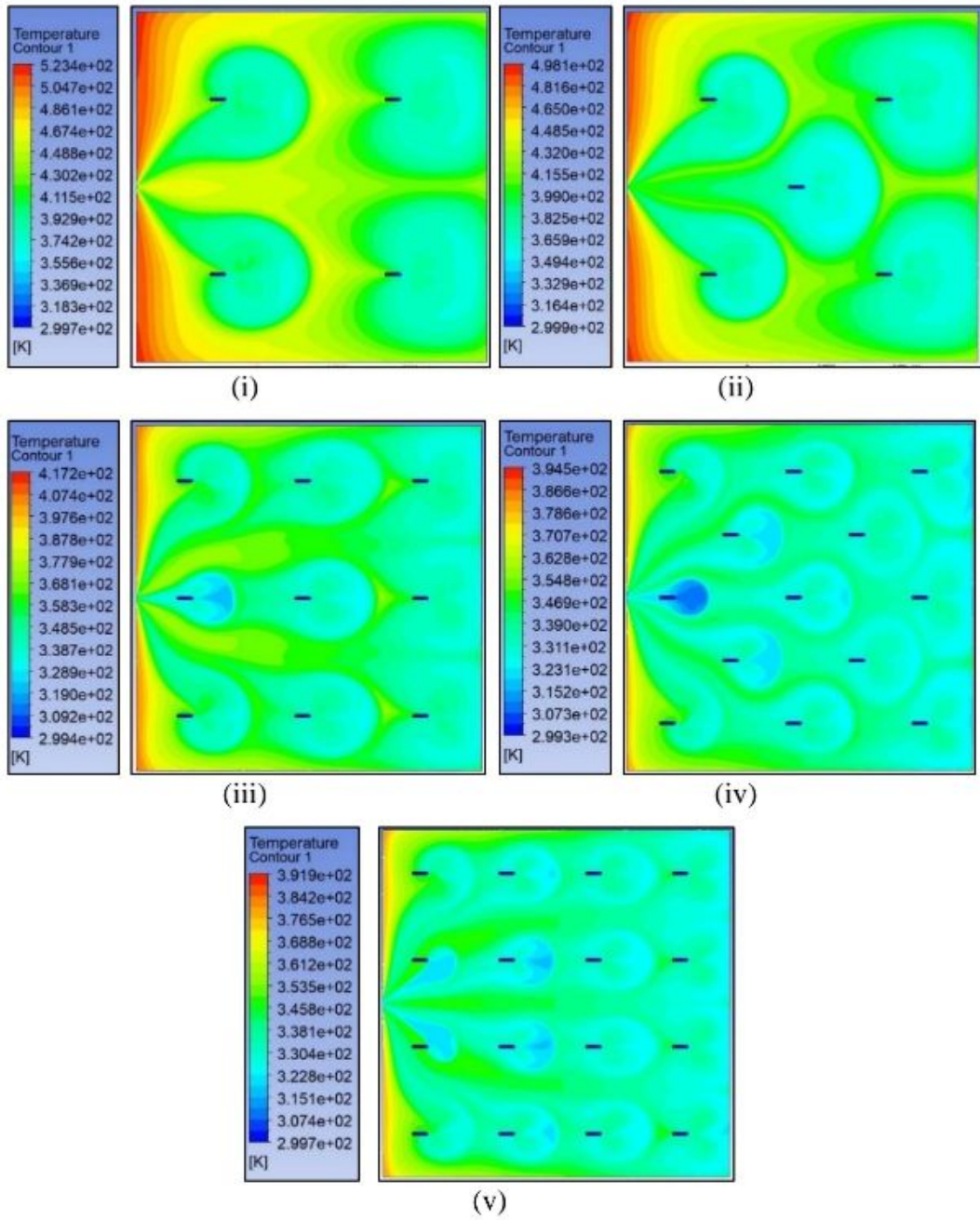


Fig. 5.1.2. Temperature Contour of Liquid Channel for E60 Hexagonal Jets
 (i) 4 hex-jets, (ii) 5 hex-jets, (iii) 9 hex-jets, (iv) 13 hex-jets, (v) 16 hex-jets

Table 5.1.2: T_{avg} of Liquid Channel for E60 design

No. of Jets	Avg. temp. of Liquid Channel
4	433.669
5	409.14
9	361.22
13	344.305
16	344.285

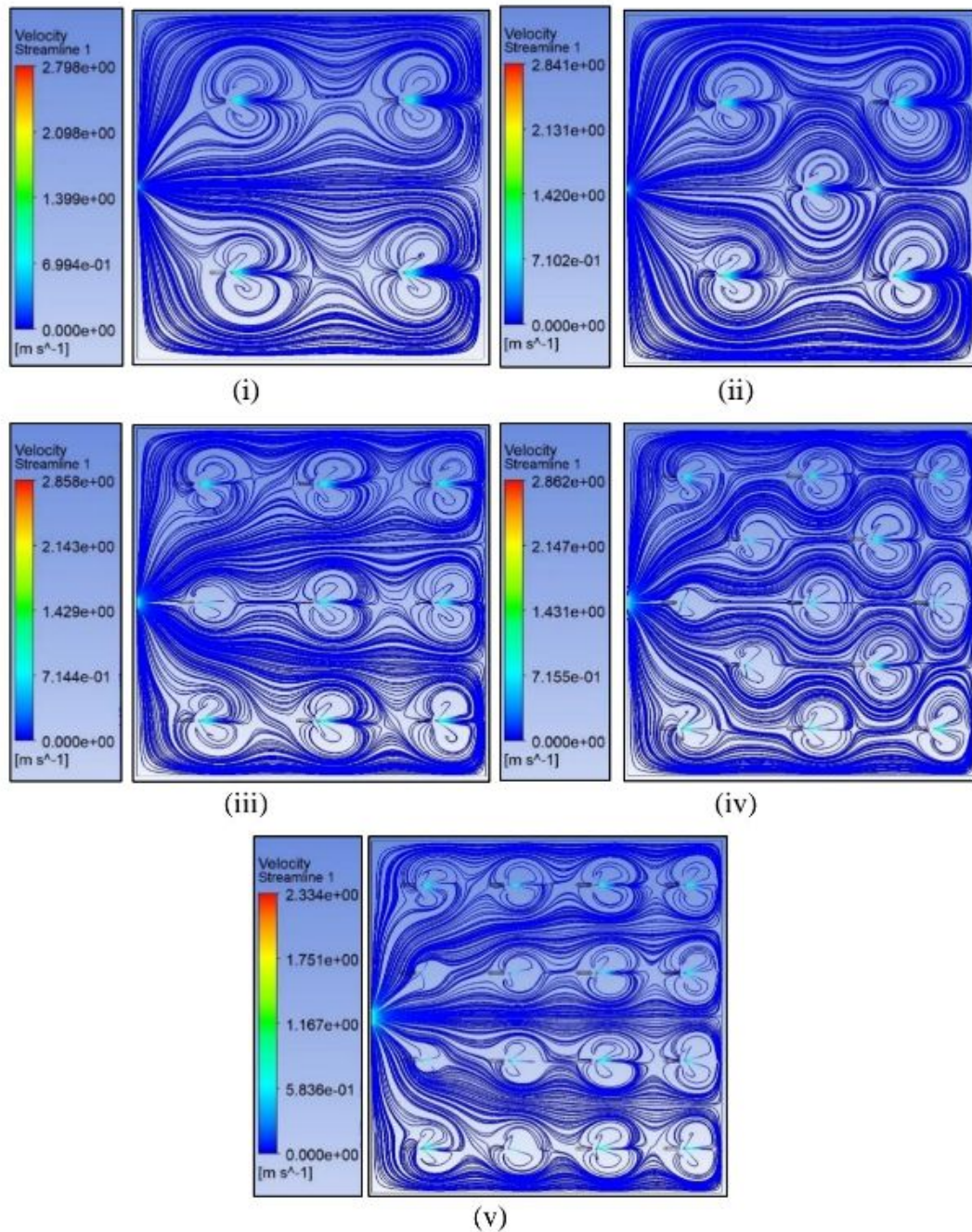


Fig. 5.1.3 Velocity Contour Streamline Distribution for E60 Hexagonal Jets
 (i) 4 hex-jets, (ii) 5 hex-jets, (iii) 9 hex-jets, (iv) 13 hex-jets, (v) 16 hex-jets

5.2 Results for E80 Hexagonal Cross-Section Micro-Jets Impingement Heat Sink for Various No. Of Jets.

Fig. 5.2.1 provides temperature contours at solid-liquid contact region of impingement heat sink for E80 hex-jets. Fig. 5.2.2 represents the temperature contour of liquid channel in impingement heat sink for E80 design models of several no. of jets. Fig. 5.2.3 shows the velocity contour where streamlines showing the movement of high velocity fluid through jet nozzles to the low velocity fluid.

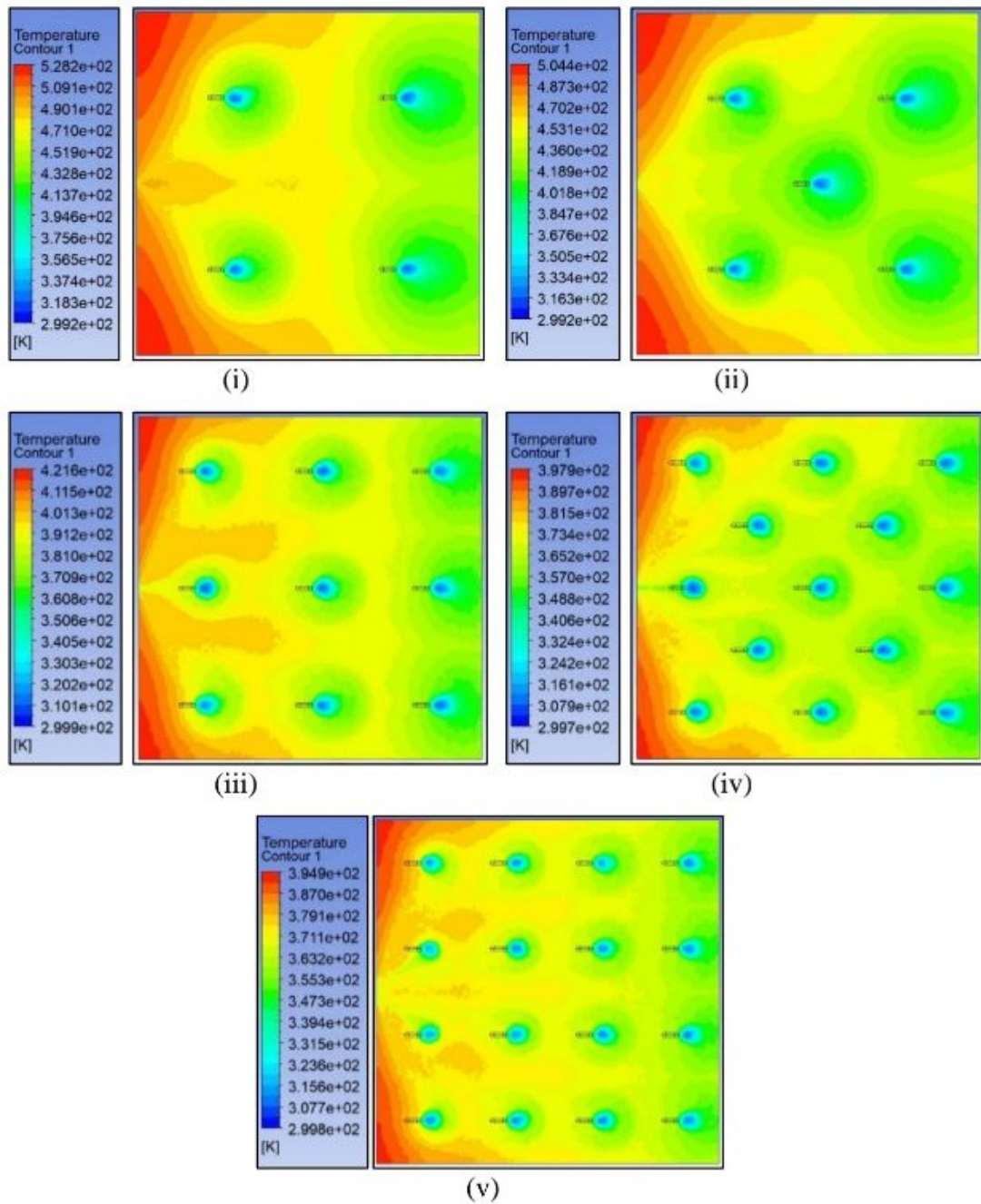


Fig. 5.2.1. Temp. Contours at Solid-Liquid Contact Region for E80 Hexagonal Jets
 (i) 4 hex-jets, (ii) 5 hex-jets, (iii) 9 hex-jets, (iv) 13 hex-jets, (v) 16 hex-jets

Table 5.2.1: The Avg. temperature of contact region of fluid and solid for E80 design

No. of Jets	Avg. temp. of contact region
4	479.164
5	454.519
9	401.715
13	382.483
16	382.646

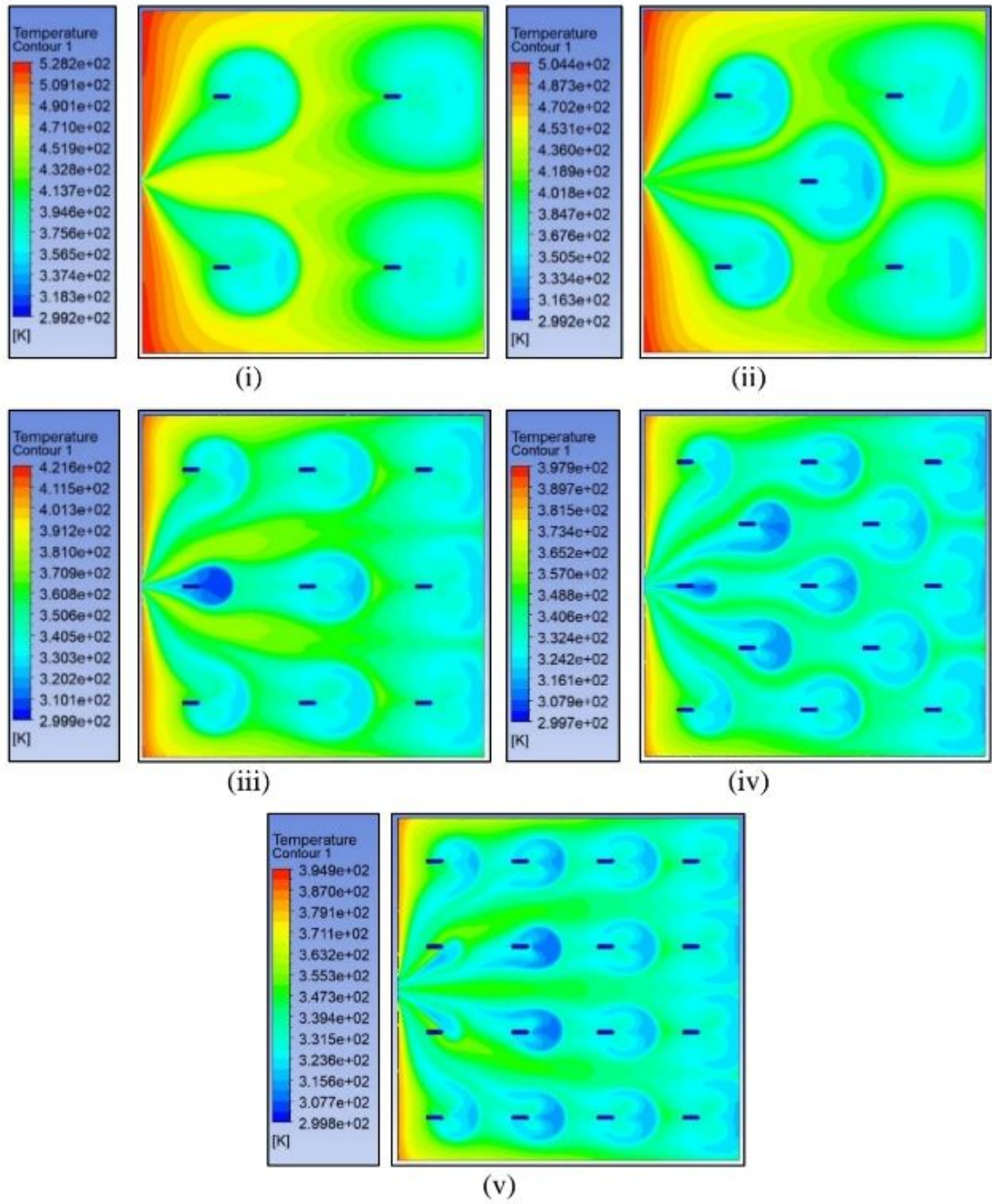


Fig. 5.2.2. Temperature Contour of Liquid Channel for E80 Hexagonal Jets
 (i) 4 hex-jets, (ii) 5 hex-jets, (iii) 9 hex-jets, (iv) 13 hex-jets, (v) 16 hex-jets

Table 5.2.2: T_{avg} of Liquid Channel for E80 design

No. of Jets	Avg. temp. of Liquid Channel
4	435.769
5	411.974
9	361.608
13	344.565
16	344.281

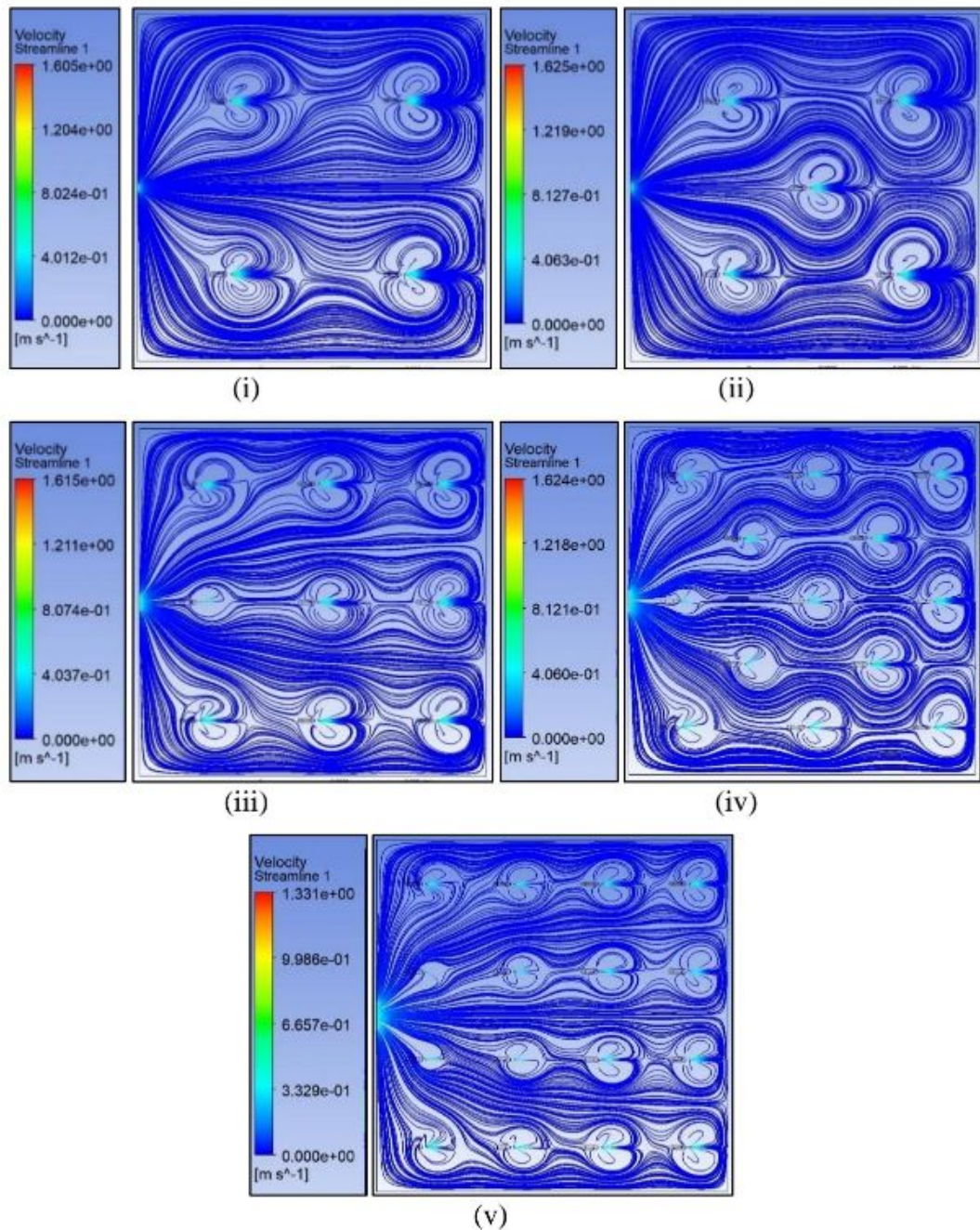


Fig. 5.2.3 Velocity Contour Streamline Distribution for E80 Hexagonal Jets
 (i) 4 hex-jets, (ii) 5 hex-jets, (iii) 9 hex-jets, (iv) 13 hex-jets, (v) 16 hex-jets

5.3 Results for E100 Hexagonal Cross-Section Micro-Jets Impingement Heat Sink for Various No. Of Jets.

Fig. 5.3.1 provides temperature contours at solid-liquid contact region of impingement heat sink for E100 hex-jets. Fig. 5.3.2 represents the temperature contour of liquid channel in impingement heat sink for E100 design models of several no. of jets. Fig. 5.3.3 shows the velocity contour where streamlines showing the movement of high velocity fluid through jet nozzles to the low velocity fluid.

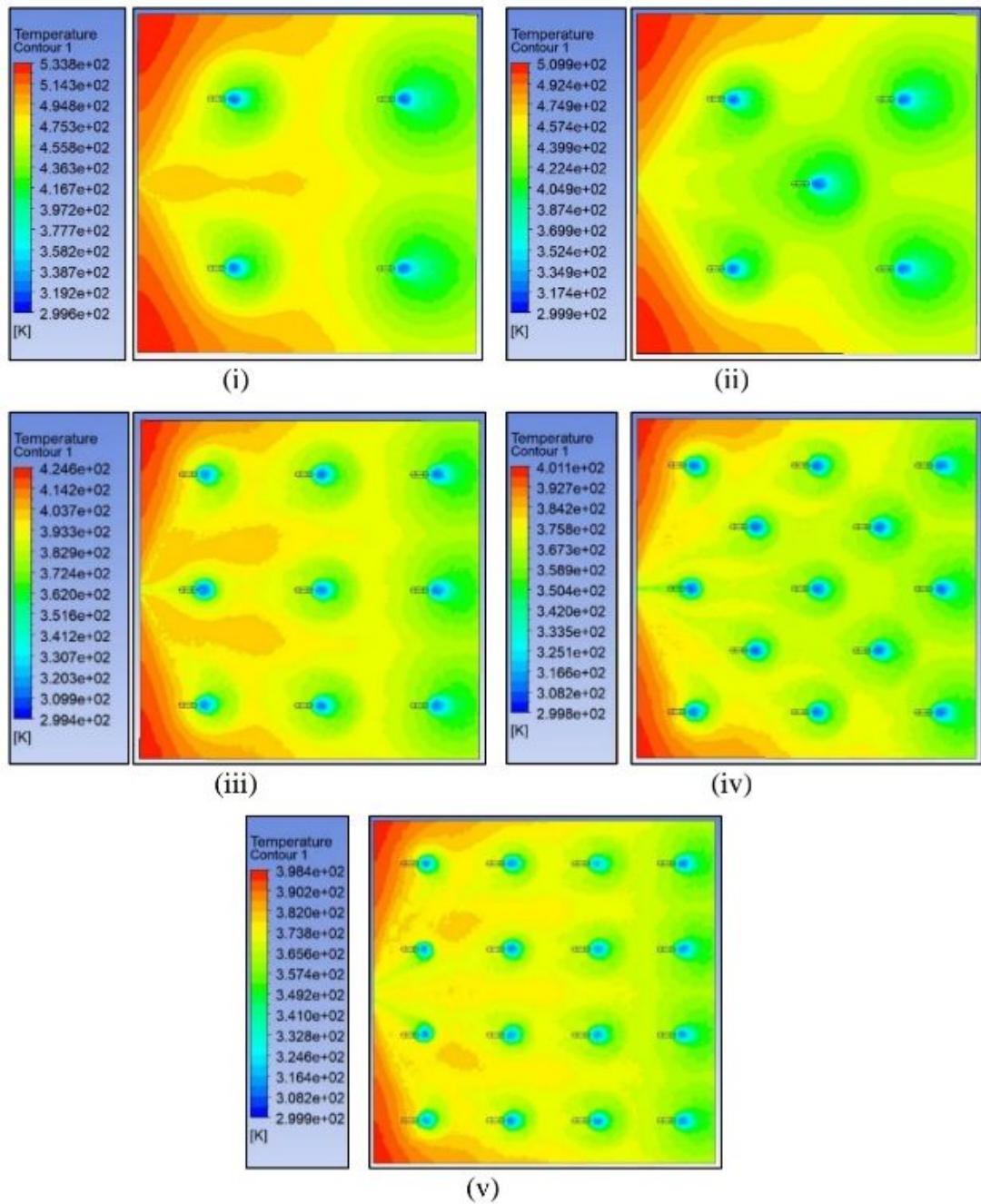


Fig. 5.3.1. Temp. Contours at Solid-Liquid Contact Region for E100 Hexagonal
 (i) 4 hex-jets, (ii) 5 hex-jets, (iii) 9 hex-jets, (iv) 13 hex-jets, (v) 16 hex-jets

Table 5.3.1: The Avg. temperature of contact region of fluid & solid for E100 design

No. of Jets	Avg. temp. of contact region
4	493.744
5	469.144
9	414.056
13	395.113
16	396.388

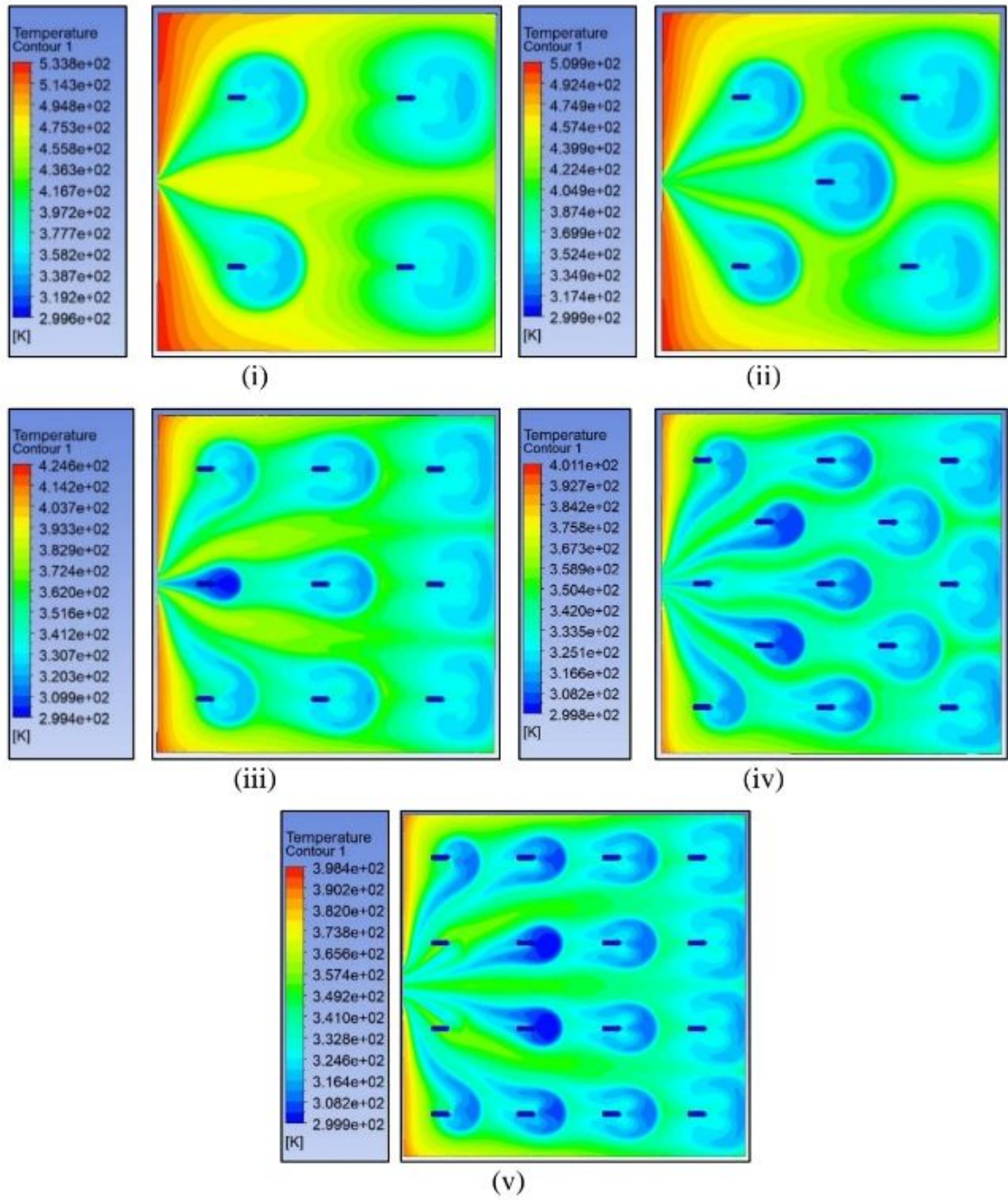


Fig. 5.3.2. Temperature Contour of Liquid Channel for E100 Hexagonal Jets
 (i) 4 hex-jets, (ii) 5 hex-jets, (iii) 9 hex-jets, (iv) 13 hex-jets, (v) 16 hex-jets

Table 5.3.2: T_{avg} of Liquid Channel for E100 design

No. of Jets	Avg. temp. of Liquid Channel
4	438.945
5	415.193
9	362.272
13	345.049
16	344.684

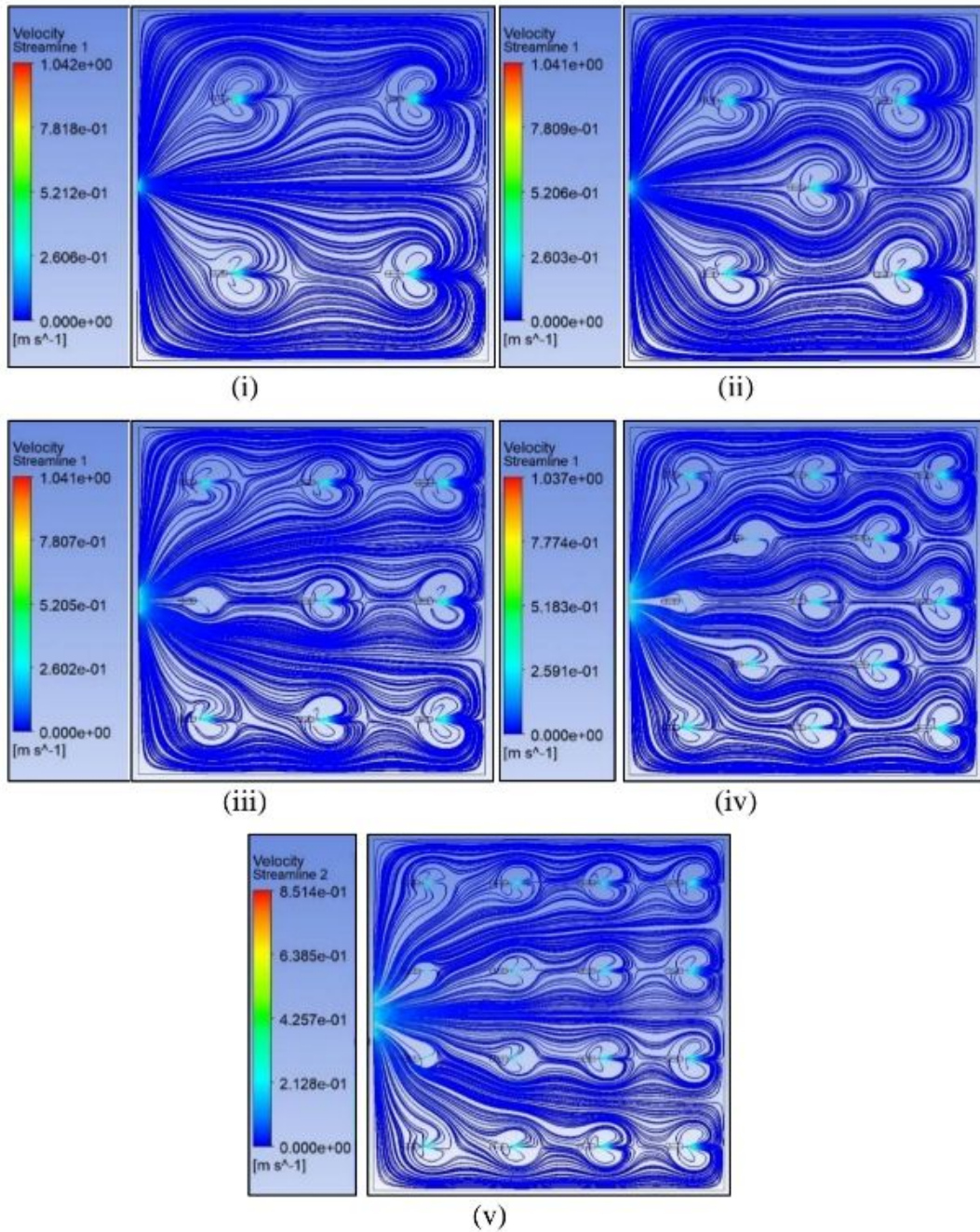


Fig. 5.3.3 Velocity Contour Streamline Distribution for E100 Hexagonal Jets
 (i) 4 hex-jets, (ii) 5 hex-jets, (iii) 9 hex-jets, (iv) 13 hex-jets, (v) 16 hex-jets

The streamline velocity contours were obtained for all the different jet configurations investigated. These contours visually depict the flow patterns and velocity distribution within the micro-jets. By analyzing the streamline velocity contours, we can get insights into the flow behaviour and identify areas of high and low fluid velocities.

The streamline velocity contours also provided insights into the impact of the number of jets on the fluid flow characteristics. Comparing the contours across

different jet array configurations, researchers were able to observe variations in the flow patterns and identify the influence of the number of jets on the velocity distribution. The streamline velocity contours provided a generalised visual representation of the fluid flow behaviour within the micro-jet impingement cooling system. They offered useful details regarding the velocity distribution, flow patterns, and problem or opportunity areas.

Successful modelling of the aforementioned jet configurations with three different design variables i.e. edge lengths and the resulting thermal parameter values, such as the average surface maximum pressure drop throughout the channel ΔP (kPa), Temperature of fluid-solid interface, and Temperature of fluid at outlet are extracted from the contour plots that are assessed in the ANSYS Fluent software. A straight forward graph that depicts the variation of these thermal characteristics in relation to the quantity of jets and various values of an is used for further investigation.

5.4 Micro-jet design parameters i.e., Edge length and no. of jets effect on the performance of the heat sink

- a) Average contact region temperature of fluid & solid, T_{avg} (K)
- b) Pressure drop variation through the channel (ΔP)
- c) Outlet temp. of fluid, T_o (K)

Fig. 5.4.1 illustrates the distinctive changes in the mean surface temp. of the fluid-solid contact zone with altering the no. of 45° angled hex-jets at a constant flow rate. It is clear from Fig. 5.4.1 that for all jet designs, the mean surface temp. of the fluid-solid contact zone declines as the number of jets varies from 4 to 16. The largest temperature drop was attained using a hex-jet of edge length 60 microns.

Fig. 5.4.2 displays an examination of the total pressure drop throughout the channel for three hexagonal cross-sections of edge length 0.06, 0.08 and 0.1 mm, where the highest-pressure loss occurs for a jet edge length of 0.06m i.e., E60 design variable. The above result indicates the smallest possible jet dimensions for building a microchannel heat sink since the heat transport constant is influenced by The reduction in pressure through the channel. As a result, when the pressure drop is at its highest, the heat transfer coefficient reaches its maximum value. This leads to enhanced heat transmission, making it more effective.

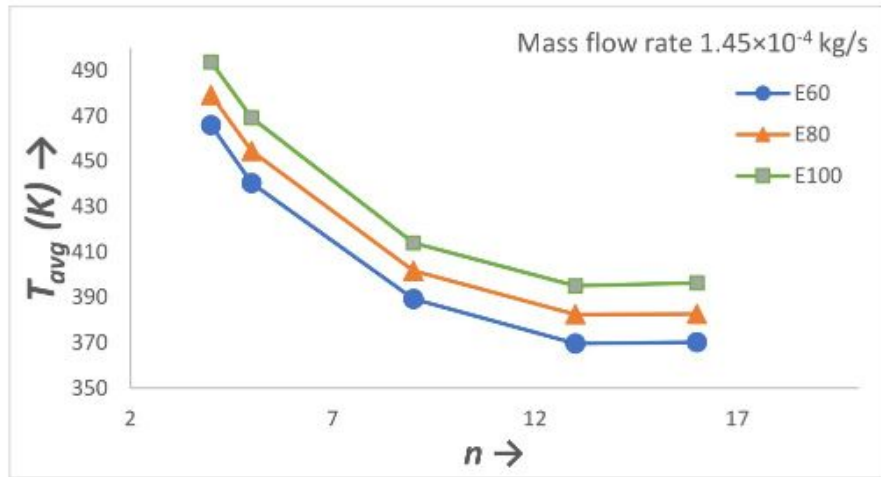


Fig. 5.4.1. Variability in temperature at the fluid-solid interface as a function of the number of 45° angled jets

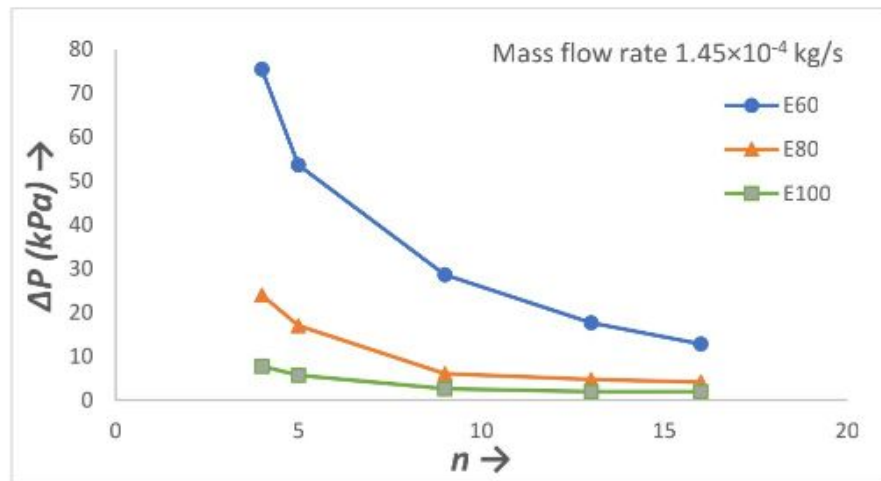


Fig. 5.4.2. Graph showing pressure variance with changing number of 45° angled Jets

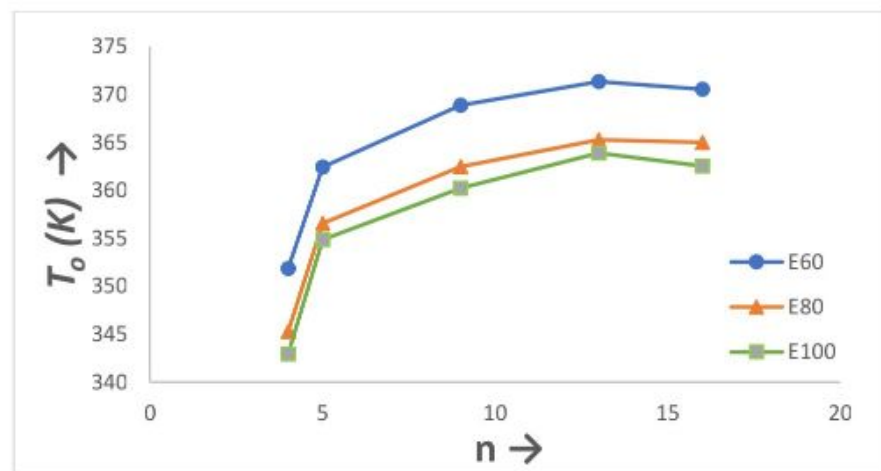


Fig. 5.4.3. Exit Temperature Fluctuation of Fluid in Relation to Altered Quantity of Angled Jets

With the increase in the T_{avg} (K) of nozzles from four to nine, The reduction in pressure within the channel and variability in temperature improve while there is a significant decrease in the mean surface temp. of the fluid-solid contact zone. This leads to good results in the rate of heat transfer. Which demonstrates the dominant stagnation heat transfer; additionally, the number of nozzles was increased from nine to sixteen, which decreased stagnation transfer and, in turn, the h_{avg} .

With increasing number of jets (n), it was found that both ΔP and average surface temperature of contact region, T_{avg} (K), significantly decreased until a staggered 9 jet array was attained. The T_{avg} (K) and ΔP only little changed as the number of micro-jets was increased from the staggered 9-jet to 13-jet heat sink array, as illustrated in fig. Even though the pressure drops monotonously, the subsequent modification of the jet arrangement from a staggered 13-jet array to an inline 16 jet array resulted in a tiny rise in T_{avg} (Kelvin). Increasing the number of jets also results in a drop in the mass flow rate per jet.

Due to the high temperatures that are attained close to the walls, the heat sink's upper walls and assumed adiabatic side have a significant impact on the uniformity of temperature distribution. Due to congestion in a fluid flow, the staggered 13-jet array demonstrated a greater reduction in T_{avg} (K) in comparison with inline 16 jet array because to the smaller gap between the two hexagonal micro-jets and the distance of the jets from the side wall.

CHAPTER 6

CONCLUSIONS

After all inceptions, simulation allowed us to draw certain inferences. An ANSYS Fluent model and solution for one pass of continuous flow of water in multiple inclined micro-jet impingement cooling mechanism have been defined in different micro-jet segment of heat sinks above.

- Through CFD simulation, the study explored the pressure and temperature variation properties of silicon-based solid substrate impingement heat sinks for cooling electronic devices.
- The inclined 13-jet model's validation was completed satisfactorily, and the validation results were compared to the experimental findings presented in [39].
- Two design parameters, namely the edge length of the hexagonal cross section and the number of jets (n), were discovered to have an impact on the heat transfer coefficient (h), pressure drop, and temperature drop, which are the three main target functions.
- The optimal nozzle angle into the impingement heat sink for high temperature decrease at the system's outlet has been determined to be a 45° angle for all micro-jets.
- For the purpose of determining the temperature and pressure-drop characteristics, simulation-based evaluation of a number of micro-dimensional jet configurations, including inclined 4 jet, 5 jet, 9 jet, 13-jet, and 16 jet heat sinks with varying jet diameters, was conducted.
- The rise in the number of jets led to greater heat transfer and temperature distribution, which in turn raised the number of jet impingements up to a point before becoming saturation. Fig. 5.4.2 illustrates how the decline in T_{avg} (K) values for the three configurations 9 jet, 13 jet, and inline 16 jet-array—was relatively similar.
- With more jets, the pressure loss across the micro-jets was reduced. This suggests that increasing the number of jets can lessen flow resistance, resulting in a decrease in energy consumption and enhanced fluid dynamics.

REFERENCES

- [1] D. B. Tuckerman and R. F. W. Pease, "High-performance heat sinking for VLSI," *IEEE Electron Device Letters*, vol. 2, no. 5, pp. 126–129, May 1981, doi: 10.1109/edl.1981.25367.
- [2] L. T. Yeh, "Review of Heat Transfer Technologies in Electronic Equipment," *Journal of Electronic Packaging*, vol. 117, no. 4, pp. 333–339, Dec. 1995, doi: 10.1115/1.2792113.
- [3] S. V. Garimella and R. Rice, "Confined and Submerged Liquid Jet Impingement Heat Transfer," *Journal of Heat Transfer*, vol. 117, no. 4, pp. 871–877, Nov. 1995, doi: 10.1115/1.2836304.
- [4] S. L. Wu, J. Mai, Y.-C. Tai, and C.-T. Ho, "Micro heat exchanger by using MEMS impinging jets." 1999. doi: 10.1109/memsys.1999.746799.
- [5] D. M. Lee and K. Vafai, "Comparative analysis of jet impingement and microchannel cooling for high heat flux applications," *International Journal of Heat and Mass Transfer*, vol. 42, no. 9, pp. 1555–1568, May 1999, doi: 10.1016/s0017-9310(98)00265-8.
- [6] X. Peng and G. P. Peterson, "Convective heat transfer and flow friction for water flow in microchannel structures," *International Journal of Heat and Mass Transfer*, vol. 39, no. 12, pp. 2599–2608, Aug. 1996, doi: 10.1016/0017-9310(95)00327-4.
- [7] K. Foli, T. Okabe, M. Olhofer, Y. Jin, and B. Sendhoff, "Optimization of micro heat exchanger: CFD, analytical approach and multi-objective evolutionary algorithms," *International Journal of Heat and Mass Transfer*, vol. 49, no. 5–6, pp. 1090–1099, Mar. 2006, doi: 10.1016/j.ijheatmasstransfer.2005.08.032.
- [8] G. M. Mala, D. Li, and J. Dale, "Heat transfer and fluid flow in microchannels," *International Journal of Heat and Mass Transfer*, vol. 40, no. 13, pp. 3079–3088, Sep. 1997, doi: 10.1016/s0017-9310(96)00356-0.
- [9] H. M. Ali and W. Arshad, "Thermal performance investigation of staggered and inline pin fin heat sinks using water based rutile and anatase TiO₂ nanofluids," *Energy Conversion and Management*, vol. 106, pp. 793–803, Dec. 2015, doi: 10.1016/j.enconman.2015.10.015.
- [10] M. Zunaid, "NUMERICAL STUDY OF PRESSURE DROP AND HEAT TRANSFER IN A STRAIGHT RECTANGULAR AND SEMI CYLINDRICAL PROJECTIONS MICROCHANNEL HEAT SINK," *Journal of Thermal Engineering*, vol. 3, no. 5, pp. 1453–1465, Sep. 2017, doi: 10.18186/journal-of-thermal-engineering.338903.
- [11] M. Zunaid, H. M. Cho, A. Husain, A. Jindal, R. Kumar, and B. S. Chauhan, "Computational Analysis of Liquid Jet Impingement Micro-channel Cooling," *Materials Today: Proceedings*, vol. 5, no. 14, pp. 27877–27883, Jan. 2018, doi: 10.1016/j.matpr.2018.10.026.

- [12] L. Lixiao et al., "Flow characteristics and heat transfer performance in a Y-Fractal mini/microchannel heat sink," *Case Studies in Thermal Engineering*, vol. 15, p. 100522, Nov. 2019, doi: 10.1016/j.csite.2019.100522
- [13] A. H. El-Shazly, S. Ookawara, A. Radwan, M. F. Elkady, and A. H. El-Shazly, "Optimization of stepwise varying width microchannel heat sink for high heat flux applications," *Case Studies in Thermal Engineering*, vol. 18, p. 100587, Jan. 2020, doi: 10.1016/j.csite.2020.100587.
- [14] W. Duangthongsuk and S. Wongwises, "An experimental investigation on the heat transfer and pressure drop characteristics of nanofluid flowing in microchannel heat sink with multiple zigzag flow channel structures," *Experimental Thermal and Fluid Science*, vol. 87, pp. 30–39, Oct. 2017, doi: 10.1016/j.expthermflusci.2017.04.013.
- [15] R. K. Ajeel, W. S.-I. W. Salim, and K. Hasnan, "Thermal and hydraulic characteristics of turbulent nanofluids flow in trapezoidal-corrugated channel: Symmetry and zigzag shaped," *Case Studies in Thermal Engineering*, vol. 12, pp. 620–635, Sep. 2018, doi: 10.1016/j.csite.2018.08.002.
- [16] W. Arshad and H. M. Ali, "Experimental investigation of heat transfer and pressure drop in a straight minichannel heat sink using TiO₂ nanofluid," *International Journal of Heat and Mass Transfer*, vol. 110, pp. 248–256, Jul. 2017, doi: 10.1016/j.ijheatmasstransfer.2017.03.032.
- [17] S. Kumar, A.D. Kothiyal, M.S. Bisht, A. Kumar, "Numerical analysis of thermal hydraulic performance of Al₂O₃-H₂O nanofluid flowing through a protrusion obstacles square mini channel," *Case Stud. Therm. Eng.*, vol. 9, no. December 2016, pp. 108–121, 2017, doi: 10.1016/j.csite.2017.01.004.
- [18] M. M. Baba, A. V. S. R. Raju, and M. S. R. Rao, "Heat transfer enhancement and pressure drop of Fe₃O₄ -water nanofluid in a double tube counter flow heat exchanger with internal longitudinal fins," *Case Studies in Thermal Engineering*, vol. 12, pp. 600–607, Sep. 2018, doi: 10.1016/j.csite.2018.08.001.
- [19] Y. Hou, J.-L. Yang, and W. Zhang, "Numerical Study of Enhanced Heat Transfer of MicroChannel Heat Sink with Nanofluids," *IOP Conference Series: Materials Science and Engineering*, Jan. 2020, doi: 10.1088/1757-899x/721/1/012052.
- [20] R. Ch. Al-Zuhairy, Z. S. Kareem, and A. A. Abdul-Hadi, "Al₂O₃-water nanofluid heat transfer enhancement of a twin impingement jet," *Case Studies in Thermal Engineering*, vol. 19, p. 100626, Jun. 2020, doi: 10.1016/j.csite.2020.100626.
- [21] P. C. M. Kumar and C. M. S. Kumar, "Numerical study on heat transfer performance using Al₂O₃/water nanofluids in six circular channel heat sink for electronic chip," *Materials Today: Proceedings*, vol. 21, pp. 194–201, Jan. 2020, doi: 10.1016/j.matpr.2019.04.220.

- [22] S. L. Wu, J. Mai, Y.-C. Tai, and C.-T. Ho, Micro heat exchanger by using MEMS impinging jets. 1999. doi: 10.1109/memsys.1999.746799.
- [23] D. M. Lee and K. Vafai, “Comparative analysis of jet impingement and microchannel cooling for high heat flux applications,” *International Journal of Heat and Mass Transfer*, vol. 42, no. 9, pp. 1555–1568, May 1999, doi: 10.1016/s0017-9310(98)00265-8.
- [24] A. G. Fedorov and R. Viskanta, “Three-dimensional conjugate heat transfer in the microchannel heat sink for electronic packaging,” *International Journal of Heat and Mass Transfer*, vol. 43, no. 3, pp. 399–415, Feb. 2000, doi: 10.1016/s0017-9310(99)00151-9.
- [25] K. Ambatipudi and M. S. Rahman, “Analysis of conjugate heat transfer in microchannel heat sinks,” *Numerical Heat Transfer Part A-applications*, vol. 37, no. 7, pp. 711–731, Jun. 2000, doi: 10.1080/104077800274046.
- [26] D. Liu and S. V. Garimella, “Analysis and optimization of the thermal performance of microchannel heat sinks,” *International Journal of Numerical Methods for Heat & Fluid Flow*, vol. 15, no. 1, pp. 7–26, Jan. 2005, doi: 10.1108/09615530510571921.
- [27] W. Qu and I. Mudawar, “Analysis of three-dimensional heat transfer in micro-channel heat sinks,” *International Journal of Heat and Mass Transfer*, vol. 45, no. 19, pp. 3973–3985, Sep. 2002, doi: 10.1016/s0017-9310(02)00101-1.
- [28] W. Qu and I. Mudawar, “Experimental and numerical study of pressure drop and heat transfer in a single-phase micro-channel heat sink,” *International Journal of Heat and Mass Transfer*, vol. 45, no. 12, pp. 2549–2565, Jun. 2002, doi: 10.1016/s0017-9310(01)00337-4.
- [29] A. Husain and K.-Y. Kim, “Shape Optimization of Micro-Channel Heat Sink for Micro-Electronic Cooling,” *IEEE Transactions on Components and Packaging Technologies*, vol. 31, no. 2, pp. 322–330, May 2008, doi: 10.1109/tcapt.2008.916791.
- [30] G. J. Michna, E. C. Browne, Y. Peles, and M. C. Jensen, “Single-Phase Microscale Jet Stagnation Point Heat Transfer,” *Journal of Heat Transfer*, vol. 131, no. 11, Nov. 2009, doi: 10.1115/1.3154750.
- [31] A. Husain, S. Y. Kim, and K.-Y. Kim, “Performance analysis and design optimization of micro-jet impingement heat sink,” *Heat and Mass Transfer*, vol. 49, no. 11, pp. 1613–1624, Jul. 2013, doi: 10.1007/s00231-013-1202-3.
- [32] M. L. De Paz and B. A. Jubran, “Numerical modeling of multi micro jet impingement cooling of a three dimensional turbine vane,” *Heat and Mass Transfer*, May 2011, doi: 10.1007/s00231-011-0819-3.
- [33] A. Husain, J. S. Kim, and K.-Y. Kim, “Performance Characterization of Laminar Flow in Multiple Microjet Impingement Heat Sinks,” *Journal of Thermophysics and Heat Transfer*, vol. 28, no. 1, pp. 133–141, Jan. 2014, doi: 10.2514/1.t4176.
- [34] T. Muszyński and R. Andrzejczyk, “Heat transfer characteristics of hybrid microjet – Microchannel cooling module,” *Applied Thermal Engineering*,

- vol. 93, pp. 1360–1366, Jan. 2016, doi: 10.1016/j.applthermaleng.2015.08.085.
- [35] A. Husain, M. Ariz, N. Al-Rawahi, and M. N. Ansari, “Thermal performance analysis of a hybrid micro-channel, -pillar and -jet impingement heat sink,” *Applied Thermal Engineering*, vol. 102, pp. 989–1000, Jun. 2016, doi: 10.1016/j.applthermaleng.2016.03.048.
- [36] P. Naphon, S. Wiriyasart, T. Arisariyawong, and L. Nakharintr, “ANN, numerical and experimental analysis on the jet impingement nanofluids flow and heat transfer characteristics in the micro-channel heat sink,” *International Journal of Heat and Mass Transfer*, vol. 131, pp. 329–340, Mar. 2019, doi: 10.1016/j.ijheatmasstransfer.2018.11.073.
- [37] R. Kempers, J. Colenbrander, W. Tan, R. Chen, and A. Robinson, “Experimental characterization of a hybrid impinging microjet-microchannel heat sink fabricated using high-volume metal additive manufacturing,” *International Journal of Thermofluids*, vol. 5–6, p. 100029, Aug. 2020, doi: 10.1016/j.ijft.2020.100029.
- [38] M. Peng, L. Chen, W.-T. Ji, and W.-Q. Tao, “Numerical study on flow and heat transfer in a multi-jet microchannel heat sink,” *International Journal of Heat and Mass Transfer*, vol. 157, p. 119982, Aug. 2020, doi: 10.1016/j.ijheatmasstransfer.2020.119982.
- [39] A. Husain, S. Y. Kim, and K.-Y. Kim, “Performance analysis and design optimization of micro-jet impingement heat sink,” *Heat and Mass Transfer*, vol. 49, no. 11, pp. 1613–1624, Jul. 2013, doi: 10.1007/s00231-013-1202-3.
- [40] M. Zunaid, A. Husain, B. S. Chauhan, and R. Sahu, “Numerical analysis of inclined jet impingement heat transfer in microchannel,” *Materials Today: Proceedings*, vol. 43, pp. 557–563, Jan. 2021, doi: 10.1016/j.matpr.2020.12.048.
- [41] C.F.X. Ansys, “Solver Theory Guide,” Ansys CFX.